



**University of Kerbala
College of Science
Chemistry Department**

**Preparation, Characterization of Iron Oxide Nanoparticles,
and use in the Removal of Eosin Yellow Dye from aqueous
solutions**

A Thesis

Submitted to the Council of the College of Science, University of Kerbala,
in Partial Fulfillment of the Requirements for the Master Degree of
in Chemistry

By

Hussein Mhawesh Mohammad

Supervised by

**Assist. Prof. Shaymaa Ibrahim
Saeed**

Prof. Dr. Luma Majeed Ahmed

2023 AD

1444 AH

بِسْمِ اللَّهِ الرَّحْمَنِ الرَّحِيمِ

﴿يَرْفَعُ اللَّهُ الَّذِينَ آمَنُوا مِنْكُمْ وَالَّذِينَ
أُوتُوا الْعِلْمَ دَرَجَاتٍ﴾

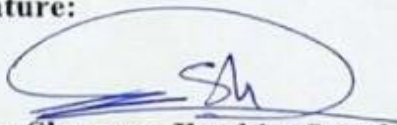
صدق الله العلي العظيم

سورة المجادلة
الآية (١١)

Supervisor Certification

We certify that this thesis, entitled "**Preparation, Characterization of Iron Oxide Nanoparticles, and Use in the removal of Eosin Yellow Dye from aqueous solutions**" has been prepared under my supervision, by "**Hussein Mhawesh Mohammad**" at the department of Chemistry, College of Science, University of Kerbala in a partial fulfillment of the requirements for the degree of Master of Science in Chemistry

Signature:



Name: Shaymaa Ibrahim Saeed
Title: Assist Professor
Address: University of Kerbala,
College of Science, Department of
Chemistry
Date: 20 / 2 / 2023

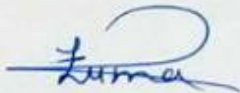
Signature:



Name: Dr. Luma Majeed Ahmed
Title: Professor
Address: University of Kerbala, College
of Science, Department of chemistry.
Date: 20 / 2 / 2023

In view of the available recommendations, I forward this thesis for debate by the examining committee.

Signature:



Name: Luma Majeed Ahmed
Title: Professor
Head of the Chemistry Department, college of science/ University of Kerbala
Date: 29 / 2 / 2023

Examination Committee Certification

We certify that we have read this thesis entitled " Preparation, Characterization of Iron Oxide Nanoparticles, and use in the Removal of Eosin Yellow Dye from aqueous solutions" as the examining committee, examined the student "Hussein Mhawesh Mohammad" on its contents, and that in our opinion, it is adequate for the partial fulfillment of the requirements for the Degree of Master in Science of chemistry.



Signature:

Name: **Dr. Alaa Frak Hussain**

Title: Professor

Address: University of Kerbala, College of Science, Department of Chemistry.

Date: 23/2/2023

(Chairman)

Signature



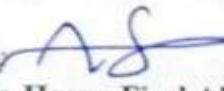
Name: **Dr. Wadhah Naji Jassim**

Title: Assistant Professor

Address: University of Baghdad ,
College of Science, Department of
Chemistry . Date: 22/2/2023

(Member)

Signature:



Name: **Dr. Hasan Faisal Al-Esary**

Title: Assistant Professor

Address: University of Kerbala, College of
Science, Department of Chemistry
Date: 20/2/2023

(Member)

Signature:



Name: **Dr. Luma M. Ahmed**

Title: Professor

Address: University of Kerbala, College
of Science, Department of Chemistry
Date: 20/2/2023

(Member & Supervisor)

Signature:



Name: **Shaymaa Ibrahim Saeed**

Title: Assistant Professor

Address: University of Kerbala, College of
Science, Department of Chemistry
Date: 20/2/2023

(Member & Supervisor)

Approved by the council of the College of Science

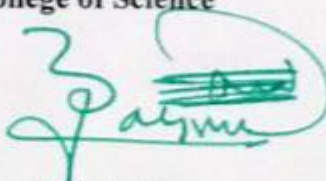
Signature :

Name: **Dr. Jasem Hanoon Hashim Al-Awadi**

Title: Assistant Professor

.Address: **Dean of College of Science, University of Kerbala**

Date: 23/2/2023



Dedication

I dedicate this work

*To my parents(My late father and my dear mother)
who have provided me with their encouragement, love,
and understanding*

*To all my extended family especially my wife Saja, my
colleagues in the plant from the heads Mr. Mahmoud
Awad , Haider Khadum and Hussein Abbas to my
brothers all QCSOs (Haider, Saad , Mohammad and
Abbas).*

*To all my friends and teachers at the University of
Kerbala*

*To all who were there for me, thank you for help me to
do my aim .To all those who have been supportive,
caring, and patient, I dedicate this simple work.*

Acknowledgments

Praise be to Allah, Lord of the worlds, May God's blessings be upon Mohammed and his pure immediate family, and thanks to God for his countless and numberless graces and gifts.

I would like to extend my deep thanks, gratitude, and appreciation to:

My supervisor Assist Prof. Shaymaa Ibrahim Saeed and Prof. Dr. Luma Majeed Ahmed for her continuous support and invaluable suggestions and great contributions since the very beginning of this work.

Also, I thank all faculty members of the Department of Chemistry in the College of Science at the University of Kerbala. Finally, I thank my family and friends for their continued support throughout this journey. They were my source of encouragement along this period.

Abstract

This work includes three routes, the first used an innovative precipitation method for creating magnetic Fe_3O_4 nanoparticles under environment oxygen without and with the use of different surfactants as templates, including sodium dodecyl sulfate (SDS), triton X100, cetrimonium bromide (CTAB), and cetramide (CT). These magnetic iron oxide (Fe_3O_4) nanoparticles were created as inverse spinel ($\text{Fe}_2\text{O}_3 \cdot \text{FeO}$), when combined iron sulfate solution with an aqueous mixture of sodium hydroxide and sodium nitrate without any calcination under oxygen gas. In second route, the prepared iron oxide nanoparticles (Spinel Fe_3O_4) were identified using several techniques, including infrared spectroscopy (FTIR), X-ray diffraction (XRD) analysis, and scanning electron microscopy (SEM). Infrared spectroscopy showed reasonable peaks at $598\text{-}744\text{ cm}^{-1}$, confirming the presence of the tetrahedral and octahedral structures of the prepared iron oxide nanoparticles as an inverse spinel. X-ray diffraction explained that the prepared samples without and with addition surfactants are crystalline in nature, with nanosize ranged (8.5 nm without surfactants to 27.72 nm with using the surfactants). SEM images of prepared iron oxide nanoparticles without and with using surfactants given spherical shapes with semi-regular clusters as Broccoli like nanostructures. On the other hand in third route, iron oxide nanoparticles were used as an adsorbent to remove eosin yellow dye from aqueous solutions. In the beginning, an adsorption experiment was conducted for all the prepared surfaces towards the dye, as it was found that the best removal percentage of the dye was on the surface of iron oxide nanoparticles with cetrimide ($\text{Fe}_3\text{O}_4 + \text{cetramide}$), where the removal percentage reached 94.7% . After that, the factors affecting the

surface adsorption process of iron oxide were studied with cetrimide only, Fe_3O_4 prepared with cetramide gave a higher removal efficiency compared with the prepared iron oxides. It was found that the adsorption capacity increased with the increase of the equilibrium time until it reached the saturation stage at a time of 60 minutes. While testing the effect of the amount of surface on the adsorption process showed an increase in the removal efficiency with the increase in the surface mass as a result of the increase in the surface area, the dye was most effectively absorbed at a weight of 0.01 g. The pH factor showed a clear effect on the removal efficiency, as it was found that the best removal of the dye in a neutral medium (pH 6.5) is due to the presence of neutralizing groups in the composition of eosin yellow dye. On the other hand, it was found that the removal efficiency increases with the increase in temperature as a result of the increase in kinetic energy, which facilitates the access of dye molecules to the active sites on the adsorbent surface. The thermodynamic study showed that the process of adsorption of iron oxide nanoparticles with cetrimide is an endothermic process since the enthalpy value is positive and spontaneous and does not require an external source, while the enthalpy value is negative and non-spontaneous in the creation of iron oxide nanoparticles without cetrimide is an exothermic process. Magnetite with cetramide obeys a chemisorption because ΔH° of this reaction is more valuable than $(20) \text{ kJ mol}^{-1}$ in opposite the Fe_3O_4 in absence cetramide is found to be Physisorption because ΔH° value is lower than $(20) \text{ kJ mol}^{-1}$. The data from the isotherm model equations show that the magnetite produced in the presence of cetramide obeys Langmuir, Freundlich, and Temkin while Fe_3O_4 produced in the absence of cetramide does not.

Table of Contents

Contents		Page
Abstract		II
Contents		IV
List of tables		VII
List of Figures		VIII
List of abbreviations and symbols		X
Chapter One: Introduction		
1.1	General Introduction	1
1.2	Adsorption Process	2
1.3	Types of Adsorption	3
1.3.1	Physical Adsorption	3
1.3.2	Chemical Adsorption	3
1.4	Adsorption from Solution	4
1.5	Adsorption Isotherms	5
1.6	Types of Isotherms	6
1.6.1	Langmuir Isotherm	7
1.6.2	Freundlich Isotherm	8
1.6.3	Temkin Isotherm	9
1.7	Thermodynamics of Adsorption	9
1.8	Using Magnetic Nanoparticles as adsorbent surfaces	11
1.9	Magnetic Bulks and Nanoparticles	12
1.10	Iron Oxide Nanoparticle	14
1.11	Methods of Synthesis of Iron Oxide Nanoparticles	16
1.11.1	Co-Precipitation Technique	16
1.11.2	Sol-Gel Technique	17
1.11.3	Hydrothermal Technique	18
1.11.4	Thermal Decomposition	19
1.12	Eosin Yellow Dye	19
1.13	Literature Survey	21
1.14	The aim of the Study	24
Chapter Two: Experimental		

2.1.1	Chemicals	25
2.1.2	Instruments	26
2.2	Preparation of Standard Solutions	27
2.2.1	Preparation of Eosin yellow dye Solutions	27
2.2.2	Preparation of Acid Solutions	27
2.2.3	Preparation of salt Solutions	27
2.2.4	Preparation of base Solutions	27
2.3	Preparation of Iron Oxide Nanoparticles	28
2.3.1	Synthesis of Spinel Fe ₃ O ₄ nanoparticles without Surfactant	28
2.3.2	Synthesis of Spinel Fe ₃ O ₄ nanoparticles with surfactant	28
2.4	Characterization of Spinal Fe ₃ O ₄	29
2.4.1	FT-IR Spectroscopy	29
2.4.2	X-Ray Diffraction Spectroscopy (XRD)	30
2.4.3	Scanning Electron Microscopy (SEM)	30
2.5	Factors Influencing the removal of the dye	30
2.5.1	Equilibrium Time	30
2.5.2	Effect of the Weight of Surface Adsorbent	31
2.5.3	Effect of pH on the dye	31
2.5.4	Effect of Temperature on the dye	31
2.6	Adsorption Isotherm	32
2.7	Equilibrium Isotherm Modeling	33
Chapter Three: Results and Discussion		
3.1	Verify the elements of the preparation equation Fe ₃ O ₄ NP	36
3.2	Characterization of Fe-oxide NPS	37
3.2.1	FT-IR spectral analysis	37
3.2.2	X-ray diffraction (XRD) analysis	38
3.2.3	Scanning electron microscopy (SEM) analysis	40
3.3	Applying Fe ₃ O ₄ NP in the Removal the Organic Contaminants	43
3.4	Using magnetic nanoparticles to remove the dye Eosin yellow	43
3.5	The efficiency of surfactant (cetramide) on created Fe ₃ O ₄ nanoparticles	46
3.6	The suggested mechanism of effect using surfactant on the adsorption	48

3.7	Study Factors influencing on Removal of Eosin yellow Dye from aqueous solution using the	50
3.7.1	Equilibrium Time of Adsorption System	50
3.7.2	Effect of the Weight of Surface Adsorbent	51
3.7.3	Effect of pH	53
3.7.4	Effect of temperature on Removal of Dye	55
3.8	Thermodynamics Parameters	57
3.9	Isotherm Models	61
3.9.1	Langmuir model	61
3.9.2	Freundlich Isotherm	62
3.9.3	Temkin Isotherm	64
3.10	Conclusions	66
3.11	Future study	68

List of Tables

No.	List of Tables	Page
1.1	Types of adsorption isotherms	6
1.2	Magnetic and physical properties of iron oxides	15
1.3	Properties of eosin yellow dye	20
2.1	Used chemicals	25
2.2	Employed instruments	26
2.3	Different isotherm models used in this study and their linear forms	33
3.1	The removal percentages of Eosin yellow dye from aqueous solutions using Fe ₃ O ₄ surface at different times and 298 K	50
3.2	Explaining Eosin dye removal percentages from aqueous solutions employing various weights from the surface of Fe ₃ O ₄ NP at 298 K	52
3.3	Eosin dye removal percentages from aqueous solutions using the surface of Fe ₃ O ₄ NP at various initial pH and at 298 K	54
3.4	Referring to Eosin dye removal percentages from aqueous solutions by using various weights from the surface of Fe ₃ O ₄ NP at 298 K	56
3.5	The kinetic and thermodynamic parameters for eosin yellow dye adsorption on Fe ₃ O ₄ surface prepared in presence and absence cetramide at (278-303) K	58
3.6	Comparing the adsorption isotherms for Fe ₃ O ₄ surfaces produced with and without cetramide	60
3.7	Compares the Fe ₃ O ₄ without and with cetramide in the Langmuir models	61
3.8	Comparative Freundlich models for Fe ₃ O ₄ without and with cetramide as the surfactant	64
3.9	Constant values of Temkin equation	64

List of Figures

No.	List of Figures	Page
1-1	Explains chemisorption and Physisorption	4
1.2	Mechanism of heterogeneous catalytic reaction	5
1-3	Diagrammatic representation of the defluorination process utilizing MNPs	12
1-4	The behavior of superparamagnetic nanoparticles with and without the existence of an applied magnetic field	14
1-5	Structure of the eosin yellow dye	21
2-1	The schematic diagram of the steps of spinal Fe ₃ O ₄ nanoparticle preparation	29
3-1	Detection of the chemicals compounds during the magnetic iron nanoparticle preparation equations such as (a) Na ₂ SO ₄ and (b) NH ₃ gas	36
3-2	The FT-IR spectra of magnetite with and without surfactants, including Fe ₃ O ₄ (a), Fe ₃ O ₄ +CT (b), Fe ₃ O ₄ +CTAB (c), Fe ₃ O ₄ +SDS (d), and Fe ₃ O ₄ +Triton X100 (e).	38
3-3	The magnetite's XRD analysis without and with its surfactants (a) Fe ₃ O ₄ , (b) Fe ₃ O ₄ +Triton X-100, (c) Fe ₃ O ₄ +Cetramide, (d) Fe ₃ O ₄ + SDS and (e)Fe ₃ O ₄ +CTAB.	40
3-4	The Scanning Electron Microscope (SEM) Spectrum of (a) magnetite without cetramide, (b) Fe ₃ O ₄ +CT, (c) Fe ₃ O ₄ +CTAB, (d) Fe ₃ O ₄ +SDS and (e) Fe ₃ O ₄ +Triton X 100.	41
3-5	(a) calibration curve for the determination of Eosin yellow dye in aqueous solution at 516 nm wavelength and (b) UV-Visible Absorption Spectrum for an Eosin yellow dye solution with concentration 6.5 mg/L	43
3-6	Relationship between produced nanoparticles with various surfactants and the E% (a) and qe (b) of dye removal at 60 minutes	45

3-7	Fe ₃ O ₄ nanoparticles in the presence of the surfactant (cetramide) are used as a mechanism to remove the dye from its solutions (adapted from the reference 87,88)	46
3-8	The five-fold elimination of dye by Fe ₃ O ₄ nanoparticles in the presence of cetramide	47
3-9	The correlation between the amount of substance that adsorbs on Fe ₃ O ₄ nanoparticle sizes in presence of a cetramide in mg/g while utilizing Fe ₃ O ₄ nanoparticle sizes in presence of a cetramide repeatedly.	48
3-10	Referring to Adsorption of the surfactant and dye on the catalyst (Fe ₃ O ₄ NP) and Micelle and Reverse Micelle Solutions Schematic, taken from this source	49
3-11	Effecting of equilibrium time on removal efficiency % of Eosin yellow dye	51
3-12	Effecting of surface weight of Fe ₃ O ₄ on clearance rate of Eosin yellow dye	52
3-13	(a) Structure of eosin in acidic and basic medium adapted and (b) Schematic for repulsion of OH groups onto iron oxide NP modified from this reference	54
3-14	Effecting of pH on the desorption of Eosin yellow dye	55
3-15	The impact of temperature on the efficacy of iron oxide nanoparticles (NP) produced in the presence of cetramide surfactant in the removal of dye (a) E % with the time (b) q _e with the time.	56
3-16	Compares the form Relationship between Eosin yellow Dye that was Generated on Fe ₃ O ₄ surface (a) in the Absence of Cetramide and (b) in the presence of cetramide as a surfactant at 1h	58
3-17	Referring to Gibb's free energy change (ΔG_0) versus temperature for (a) Fe ₃ O ₄ with cetramide (b) magnetite without cetramide	59
3-18	Plots of the Langmuir equation for Fe ₃ O ₄ NPS in (a) and Fe ₃ O ₄ NPS in (b) the presence of cetramide	62
3-19	Plots of the Freundlich Equation for Fe ₃ O ₄ NPS in (a) and Fe ₃ O ₄ NPS with cetramide in (b).	63
3-20	Plots of the Temkin Equation for Fe ₃ O ₄ NPS in (a) and Fe ₃ O ₄ NPS	65

	with Cetramide in (b).	
--	------------------------	--

List of abbreviations and Symbols

Abbreviation	The Meaning
A	Absorption
C_e	The equilibrium concentration
CTAB	Cetrimonium bromide
CT	Cetramide
D	The crystallite size of the particle
E%	The percentage of dye removal
ΔG	The change in free energy
ΔH	The heat of adsorption
JCPDS	Joint Committee on Powder Diffraction Standards
K	The equilibrium constant
K	The Scherer constant
K_f	Empirical Freundlich constant
K_L	The Langmuir isotherm constant
K_T	The equilibrium binding constant
Q_e	The amount of solute adsorbed
R	The gas constant
ΔS	The change in entropy
SDS	Sodium dodecyl sulfate
SEM	Scanning Electron Microscopy
XRD	X-Ray Diffraction Spectroscopy
β	Full-Width Half- maxima
θ	Bragg angle
λ	Wavelength of X-ray

Chapter One: Introduction

**Chapter One
Introduction****1.1. General Introduction**

The term "pollution" refers to any unfavorable or harmful environmental alteration brought on by the physical, chemical, or biological byproducts of human industrial or social activity [1]. Rivers, seas, the atmosphere, and the soil can all be impacted by pollution. Both biodegradable contaminants, like sewage effluent, which if properly treated and dispersed causes no long-term harm, and non-biodegradable contaminants, such as some industrial colors, phenol and its derivatives, organic compounds, and heavy metals (such as Pd, Cd, Cu, Cr, and Zn) in some industrial effluents can contaminate water [2, 3]. Harmful substances in water pose a major threat to both human health and the environment. The first contaminant to be noticed in water is color; therefore, before was released into water bodies, wastewater must be treated. Wastewater produced by the textile, rubber, paper, plastic, cosmetics, and dye production industries, among others, is mostly colored by residual dyes[4].These excess dyes shouldn't be released into waterways because it's unsightly and harmful to the ecosystem. Strong dye colors have the ability to block light, slow down photosynthetic activity, stop the growth of biota, and chelate metal ions, which can be micro-toxic to organisms. Due to their complicated structures and synthetic origins, dyes cannot be easily removed by standard wastewater treatment techniques because most are stable to photo agents and bio agents [5, 6].The dyes are organic substances that are soluble, especially those that belong to the groups of acids, bases, reactive, and directs. They are difficult to remove using conventional methods because they are highly soluble in water[7]. One of its properties is the ability to color a

certain substrate since it has chromophore groups in its molecular structures. However, the material capacity to fix its color is due to the auxotrophic groups, which are polar and may interact with polar groups of textile fibers [8]. The use of treatment methods utilizing physical, chemical, and biological technologies in order to preserve the sustainability of the environment for future generations is therefore imperative. It has been noted that, despite being effective, physical-chemical methods come at a significant expense in terms of electricity, inputs, or operation, as well as inconveniences caused by sludge disposal [9]. Many physical and chemical techniques have been studied to treat pollution, including ion exchange electrocoagulation and sedimentation, infiltration and reverse uniformity, chlorine treatment, and adsorption. Due to its high effectiveness and low cost in treating polluted water, adsorption is among the approaches that are most crucial [10].

1.2. Adsorption Process

Adsorption is a chemical and physical process that has enormous potential for creating high-quality effluent. This phenomenon of adsorption is basically due to the presence of residual forces at the surface of a liquid or a solid [11]. It is because of these residual forces that the substances stick to the surface and thus create an excessive concentration at the surface. Since adsorption is a spontaneous process, it is achieved via a reduction in the system free energy and a decrease in entropy [12]. This is a direct result of the fact that molecules at the surface are more organized than those in solution. The bonding that holds the adsorbate and adsorbing surface together is caused by a variety of very distinct types of forces, including dispersion forces, dipole interactions, and valence forces [13].

1.3. Types of Adsorption

Based on attractive forces operating between adsorbent and adsorbate, adsorption has been classified into two types, van der Waals adsorption (or physical adsorption), and chemisorption (or activated adsorption).

1.3.1. Physical Adsorption

Physical adsorption is a result of forces known as van der Waals forces, which are the same ones responsible for the condensation of gases into liquids. Adsorption heat should fall within the range of condensation heat, which is 20 kJ mol^{-1} or less. Physical adsorption can be easily reversed and reaches equilibrium relatively quickly when it occurs at low temperatures. Additionally, this adsorption type is general in nature and may involve many adsorbate layers on the adsorbent surface [14, 15].

1.3.2. Chemical Adsorption

The partial or total transfer of electrons between the adsorbate molecules and the adsorbent surface causes the forces implied by chemisorption. Compared to physical adsorption, the heat of adsorption is substantially greater (more than around 80 kJ/mol). Chemisorption is defined by its specificity and can be quick or slow. It can happen at room temperature or at greater temperatures and is typically irreversible in nature [16, 17].

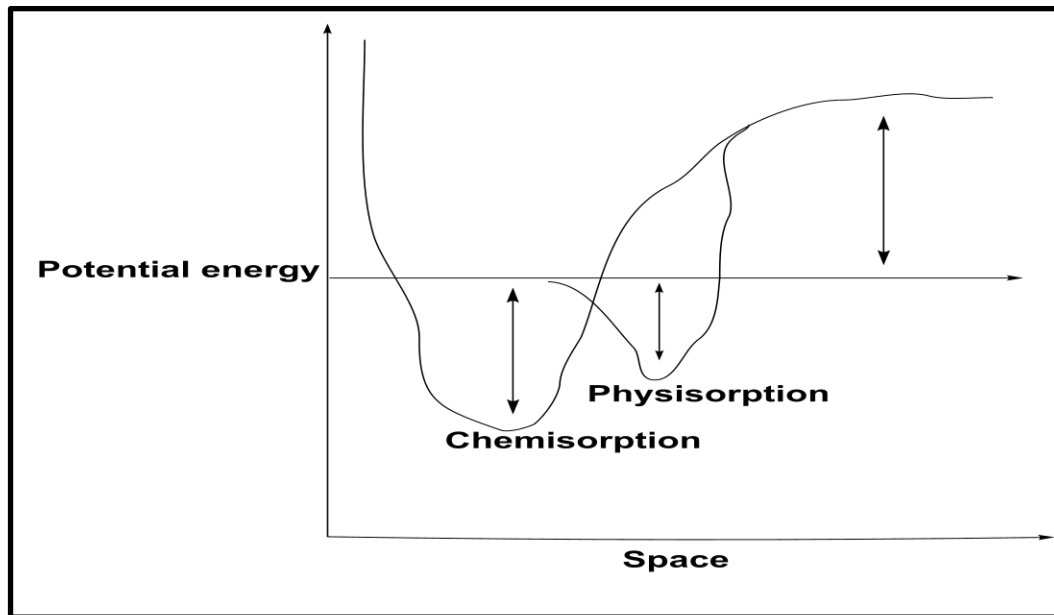


Figure (1.1) explains chemisorption and Physisorption

1.4. Adsorption from Solution

Adsorption of substances from solutions onto solid adsorbents is a rather complicated phenomena; it is distinct from the adsorption of single substances (gases, vapours, and pure liquids) in that the solution contains at least two components that create a densely packed layer on the surface. As they approach the surface's active areas, the solvent and solute molecules engage in competition. The type of interactions between the solute and the solvent in the solution phase, at the interface, and in contact with the adsorbent all play a role in this phenomenon. Adsorption from solution by porous adsorbents can be thought of as occurring primarily in four stages [18]:

- A.** Movement of solute molecules from the solution interior to the adsorbent's surface.
- B.** Adsorption onto external surface sites and solute molecule motion across the interface.

- C. Interaction of solute molecules with the sites present on the surfaces inside the adsorbent, enclosing the pore and capillary gaps.
- D. Desorption of the products from the surface.
- E. Diffusion of the products away from the surface.

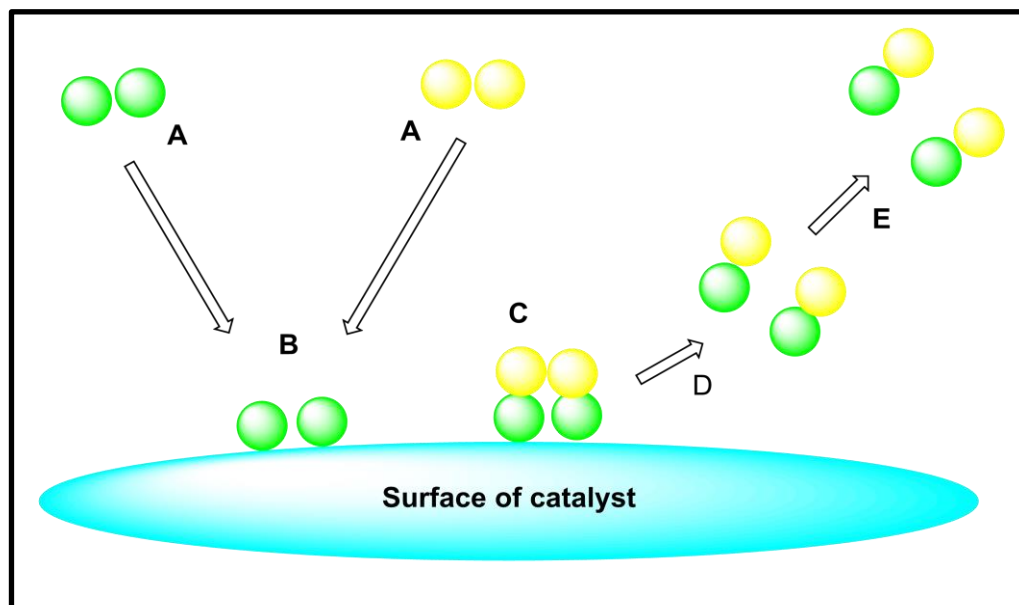


Figure (1.2) shows mechanism of heterogeneous catalytic reaction

The amount of solute that is adsorbed onto the solid particle and the rate at which it is done so may be influenced by one or more of the earlier processes. Two alternative physical representations of the adsorption of nonelectrolytes at the solid-solution interface can be used to understand it. According to this perspective, a partition between a bulk and the interfacial phase corresponds to adsorption from the solution [19].

1.5. Adsorption Isotherms

The term "adsorption isotherm" refers to the quantitative relationship between the quantity of a substance adsorbed and the equilibrium concentration of the adsorbate at a fixed temperature. By

measuring the amount of solute adsorbed (Q_e) on the surface of the solid as a function of the equilibrium concentration (C_e) of the solute in solution, the adsorption isotherm may be derived experimentally. There are many different shapes for adsorption isotherms. The adsorption mechanism and kind of adsorption can be determined by the shape of the adsorption isotherm.

Typically, it is believed that adsorption from a solution is a continuous function of the solution concentration. The shape of the isotherm of adsorption from solution is affected by intricate molecular interactions of the solution constituents with the adsorbent and with one another in surface and bulk solutions. Adsorption selectivity is low if the way the components of the solution interact with the adsorbent is similar[20].

1.6. Types of Isotherms

Different isotherms have been established theoretically or empirically. The best known are shown in Table (1-1).

Table (1.1): Types of Adsorption Isotherms

Isotherm	Applications
Langmuir	Physical and Chemical Adsorption
Freundlich	Physical and Chemical Adsorption
Temkin	Chemical Adsorption
Fowler	Physical and Chemical Adsorption
BET	Multimolecular physical adsorption

Since the Langmuir, Temkin, and Freundlich isotherms are seen to be the most pertinent isotherms in adsorption from solution, they will be covered in detail[21].

1.6.1. Langmuir Isotherm

In 1916, Langmuir presented a model for the adsorption process, and in particular for the chemisorption process, which allowed him to derive an adsorption isotherm in a straightforward but crucial theoretical way. Langmuir considered the surface of a solid to be made up of active sites each of which could adsorb one adsorbate molecule (gas molecule). Furthermore, it was assumed that all the active sites are energetically equivalent and the ability of the adsorbates to bind to the surface is independent of each other. Adsorption usually occurs till equilibrium is attained where the rate of adsorption is equal to the rate of desorption. Because Langmuir adsorption is monomolecular, it excludes the possibility of further adsorption on the adsorbate currently present on the surface [22].

In the case of adsorption from solution, Langmuir isotherm is applied in an almost similar way for the adsorption of gases on solid surfaces. Only a monolayer is still capable of adsorption, but in this case a competitive adsorption is considered to take place between the two components of solution (solute and solvent molecules). The Langmuir isotherm can be expressed as follows:

$$q_e = \frac{q_m K_L C_e}{1 + K_L C_e} \quad (1 - 1)$$

Where q_e : the amount of adsorbate adsorbed per unit weight of adsorbent at equilibrium (mg.g^{-1}). C_e : equilibrium concentration of adsorbate in solution after adsorption (mg.L^{-1}). q_m (mg.g^{-1}) is the maximum adsorption capacity, and K_L (L.mg^{-1}) is the Langmuir isotherm constant. The

equation is linearized to determine the Langmuir isotherm constants (1-2).

$$\frac{C_e}{q_e} = \frac{1}{K_L \times q_m} + \frac{C_e}{q_m} \quad (1-2)$$

As a result, by plotting C_e/q_e against C_e , one may determine K_L value from the intercept and q_m value from the slope [23].

1.6.2. Freundlich Isotherm

Freundlich puts up an empirical equation for adsorption in solution in 1926, his idea was supported by measurements from experiments. Assuming a heterogeneous surface with adsorption on each class of sites obey the Langmuir equation. The binding energy varies continuously from site to site on the solid surface, so the affinity of these sites toward the same molecule is different. Freundlich isotherm may be expressed as:

$$q_e = k_f C_e^{1/n} \quad (1-3)$$

Empirical Freundlich constant (k_f), also known as the capacity factor ($L \cdot g^{-1}$), and heterogeneity factor ($1/n$). By calculating the logarithms of equations (1-3), the Freundlich expression can be converted into a linear form:

$$\log q_e = \log k_f + \frac{1}{n} \log C_e \quad (1-4)$$

The $\log q_e$ was plotted vs. $\log C_e$, the intercept value is equal to k_f and the slope is equal to $1/n$ [24, 25].

1.6.3. Temkin Isotherm

Adsorbing species-adsorbent interactions are specifically taken into account via a component in the Temkin isotherm. This isotherm (i) is

predicated on the assumptions that I the heat of adsorption of every molecule in the layer decreases linearly with coverage as a result of adsorbent-adsorbate interactions and (ii) the adsorption is characterized by a uniform distribution of binding energies up to maximum binding energy [26]. Temkin isotherm is represented as:

$$qe = B \ln (K_T \cdot Ce) \quad (1 - 5)$$

K_T : The equilibrium binding constant ($L \cdot g^{-1}$). The Temkin isotherm constant (B), can be determined as follows:

$$B = R \cdot \frac{T}{b} \quad (1 - 6)$$

R is the gas constant ($8.314 \text{ J} \cdot \text{mol}^{-1} \cdot \text{K}^{-1}$), b is connected to the heat of adsorption ($\text{J} \cdot \text{mol}^{-1}$), and T is the absolute temperature (K). Can rearrange equation (1-5) to get the equation linear form:

$$qe = B \ln K_T + B \ln Ce \quad (1 - 7)$$

The values of b and K_T can be derived from the slope and intercept of a plot of q_e vs. $\ln C_e$, respectively[27].

1.7. Thermodynamics of Adsorption

The thermodynamic treatment of adsorption makes it possible to gather useful data on the adsorption process's randomness, spontaneity, and binding strength. Adsorption isotherms at various temperatures in

systems with reversible behavior can be measured to identify the thermodynamic functions that characterize adsorption from solution. The examination of variations in solution density, variations in the solubility of substances with temperature, etc. is obviously a necessary prerequisite of adsorption studies at various temperatures (which leads to the calculation of thermodynamic data and their interpretation) [28].

Analysis of the heat effects that come along with adsorption is one of the main goals of adsorption thermodynamics. It is not as easy to understand the heat change that takes place when a solution comes into contact with a solid as it is to understand the heat of adsorption that develops when a single gas is absorbed by a solid. It is possible to determine the heat of adsorption from solutions by measuring the concentrations needed to achieve a certain quantity of adsorption at various temperatures. The heat of adsorption from solutions is often several times lower than that of the same adsorbent from a gaseous phase [29]. Thus, the following equation could be used to calculate the heat of adsorption (ΔH) [30]:

$$\ln X_m = \frac{-\Delta H}{RT} + \text{constant} \quad (1-8)$$

Here X_m (K_{eq}) represents the maximal adsorption uptake at a certain equilibrium concentration (C_e), which was assumed to be the same across all study temperatures. Consequently, from plotting $\ln X_m$ against $1/T$, a straight line with a slope of $-\Delta H/R$ results are obtained.

Equilibrium is reached more slowly in the case of adsorption from solutions than from the gas phase. The following equation was used to determine the equilibrium constant (k_{eq}) for the adsorption process at each temperature [31] :

$$k_{eq} = \frac{q_e \cdot m(g)}{C_e \cdot V(L)} \quad (1-9)$$

Where: m is the weight of the adsorbent (g), Q_e is the amount adsorbed in mg/g, C_e is the equilibrium concentration of the adsorbate given in mg/L, and V is the volume of the adsorbate solution (L). The change in free energy (ΔG) can be calculated from equation [31, 32]:

$$\Delta G^o = -RT \ln k_d \quad (1-10)$$

Where R is the universal gas constant (J/mol K) and T is the absolute temperature in, was used to compute the Gibbs energy ΔG^o

$$k_d = \frac{C_{ads.}}{C_e} \quad (1-11)$$

The change in enthalpy ΔH^o and change in entropy ΔS^o were determined by using the Van't Hoff equation.

$$\ln k_d = \frac{-\Delta H^o}{RT} + \left(\frac{\Delta S^o}{R} \right) \quad (1-12)$$

On the other hand, using equation (1-14), the activation energy was determined [31, 33].

$$E_a = \Delta H^o + RT \quad (1-13)$$

Plotting $\ln k_d$ vs. $1/T$ yields a straight line with a slope of $-\Delta H/R$ and an intercept of $\Delta S/R$; ΔG can be calculated using the Gibbs equation [34].

1.8. Using Magnetic Nanoparticles as adsorbent surfaces

The last developments in nanotechnology have made it possible to purify water effectively. Water filtration uses various nanoparticle-based products, including carbon nanotubes, nanoscale metal oxides, nanofibers, etc. The benefit of surface modification for focusing on a

specific pollutant for adsorption and magnetic separation provided by the magnetic nanoparticles makes the procedure simple overall (Figure 1). In groundwater remediation, particularly for the removal of arsenic, the use of magnetic nanoparticles (magnetite Fe_3O_4) for separating water pollutants has already been developed. Magnetism has been used as active material in a variety of water treatment technologies, for example, coagulation, adsorption, factory pipelines, and biological processes.

Due to its extraordinarily small size and high surface-to-volume ratio, Fe_3O_4 NPs as an adsorbent surface might offer better kinetics for the adsorption of contaminants[35].

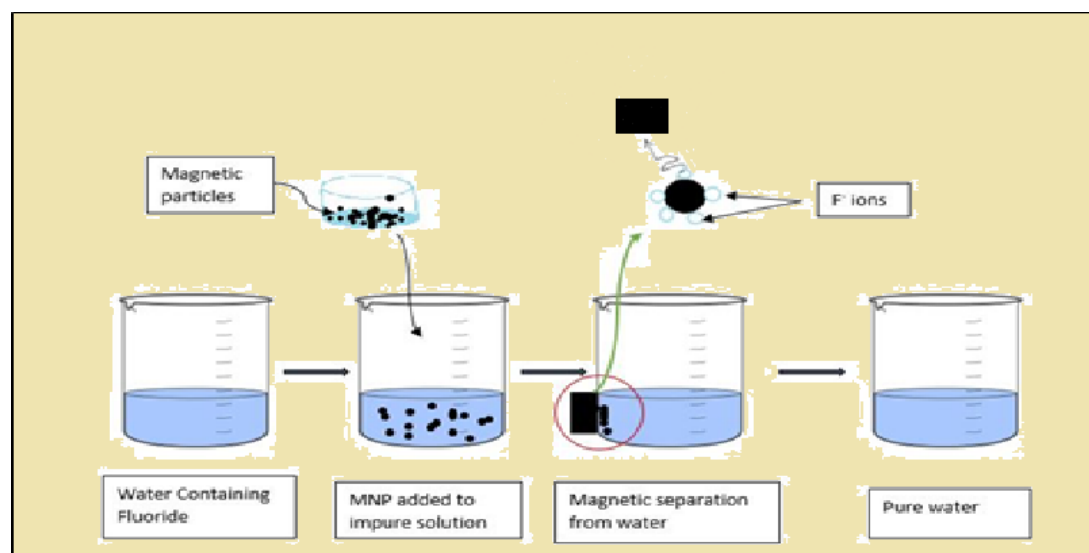


Figure (1.3): Diagrammatic representation of the defluorination process utilizing MNPs

1.9. Magnetic Bulks and Nanoparticles

Most of the features of nanoparticles compared to their bulk counterparts are the existence of a large proportion of atoms at the surface of the particle and quantum size effects. This is the reason behind the behavior of materials at the nanoscale and in turn affects the chemical reaction and the magnetic, optical, and electronic properties of the

nanoparticles[36]. Among the many various nanoparticles, magnetic bulk and nanoparticles are a derivative class of nanoparticles modified using an external magnetic field (H) of diameters ranging (100-2500) nm. For example, cobalt, iron, gold, copper, silver, and nickel[37]. The method of synthesis and chemical composition are important factors that control the physical and chemical properties of magnetic nanoparticles. The most advantages of magnetic nanoparticles are their small size, the effective surface that can be modified, large surface area, less toxicity, and superparamagnetic. The morphology is a factor influencing the magnetic properties attributable to the dominant influence of anisotropy on magnetism[38]. Superparamagnetic is a distinctive feature of nanoparticles. When shed an external magnetic field, the magnetic moments travel in the direction of the magnetic field. As the magnetic field is removed, becomes moments irregular due to the thermal energy, thus the nanoparticles lose the magnetic response. Hence, magnetic nanoparticles can be simply removed from target compounds such as biological and environmental samples with using an external magnetic field (Fig.1-2)[39]. Due to the attractive properties of magnetic particles, they have become widely used in many applications, for example cation sensors, biomedicine, environmental treatment, magnetic resonance imaging, defect sensor, nanofluids, data storage, and optical filters[40]. The instability of the magnetic nanoparticles in the reaction solution is cause by the agglomeration of the particles, as well as the loss of the magnetic and scattering property of being chemically active and oxidizing in the air. Many literatures have indicated the addition of a protective and stabilizing factor for magnetic nanoparticles. This is done through surface modification methods that include either grafting or coating using organic compounds such as surfactants and polymers, and inorganic compounds such as silica, carbon, and minerals[41].

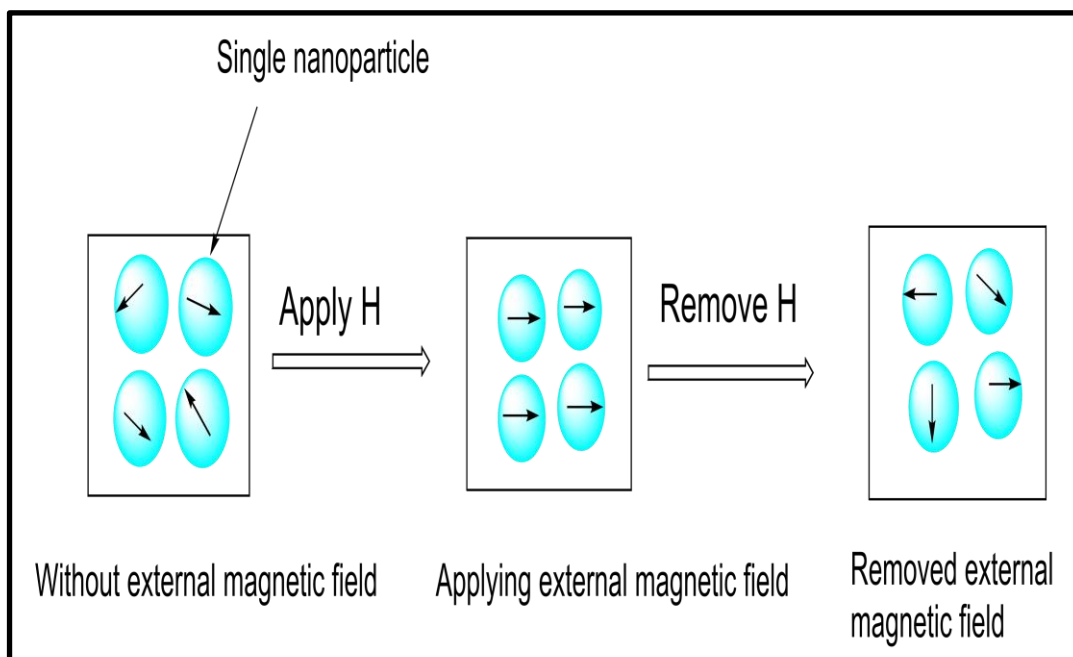


Figure (1.4): The behavior of superparamagnetic nanoparticles with and without the existence of an applied magnetic field.

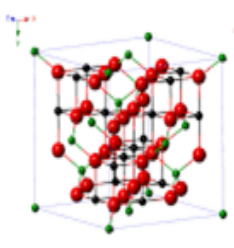
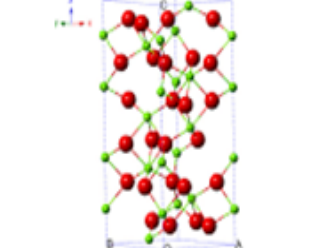
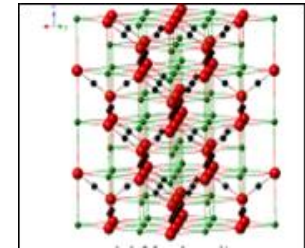
1.10. Iron Oxide Nanoparticle

The iron is the most recent transitional mineral and the main component of the earth's crust, compared to the transition elements in the same group. Iron compounds are chemically formed by combining the oxygen element with the iron element to form iron oxides. These substances are frequently employed in biological and geological applications [42]. Iron oxide appears in many forms with a crystalline structure and different magnetic and structural properties, which are hematite ($\alpha\text{-Fe}_2\text{O}_3$), magnetite (Fe_3O_4), and maghemite ($\gamma\text{-Fe}_2\text{O}_3$) as shown in Table (1.2). The crystal structures of oxide form tetrahedral and octahedral can be represented by close-packed planes of iron cations and oxygen anions[43]. The crystal structure of hematite includes a hexagonal arrangement of oxygen ions, and the octahedral sites are filled with iron ions (III). Whereas the crystal structure of magnetite and maghemite is almost similar, the cubic arrangement of the oxygen ions appears, while

the iron ions (III) have a random distribution between the octahedral and tetrahedral locations, and the iron ions (II) occupy the octahedral locations, so the final form is a cubic inverse spinel structure. Iron oxide nanoparticles have high oxidative stability, superparamagnetic properties, biocompatibility, and non-toxicity[44]. Therefore, it attracted researchers' interest due to its effective role in many fields such as wastewater treatment, catalysts, high-density data storage fields, lithium-ion batteries, modified anti-corrosive coatings, Ferro fluids and super capacitors, electrode materials, bio separations, and the separation of biochemical products. Also, the low toxicity of iron oxide nanoparticles makes them applicable in the medical field such as diagnostic magnetic resonance imaging (MRI), thermal therapy, tissue-specific releasing of therapeutic agents, magnetic sensing probes for in-vitro diagnostics (IVD), hyperthermia-based cancer treatments, and drug delivery[45].

Table (1.2): Magnetic and Physical Properties of Iron Oxides[46]

Property	Iron oxides		
	Magnetite	Hematite	Magnetite
Molecular formula	Fe ₃ O ₄	α-Fe ₂ O ₃	γ-Fe ₂ O ₃
Hardness	5.5	6.5	5
Density (g/cm ³)	5.18	5.26	4.87
Melting point (°C)	1583-1597	1350	--
Type of magnetism	Ferromagnetic	Weakly ferromagnetic or antiferromagnetic	Ferrimagnetic
Standard free energy of formation ΔG _f ^o (kJ/mol)	-1012.6	-742.7	-711.1
Color	Black to Dark Gray	rust-red	Brown, bluish black; brown to yellow
Curie temperature (K)	850	956	820-986
Space group	Fd3m	R3c (hexagonal)	P4 ₃ 32 (cubic); P4 ₁ 2 ₁ 2
Structural type	Inverse spinel	Corundum	Defect spinel

Crystallographic system	Cubic	Rhombohedral, hexagonal	Cubic or tetrahedral
Lattice parameter (nm)	$a = 0.8396$	$a=0.5034, c=1.375$ (hexagonal) $a_{Rh} = 0.5427, \alpha = 55.3^\circ$ (rhombohedral)	$a = 0.83474$ (cubic); $a = 0.8347, c = 2.50$ (tetragonal)
Structures			

1.11. Methods of Synthesis of Iron Oxide Nanoparticles

The common synthesis methods include the co-precipitation method, sol-gel method, hydrothermal technique and thermal decomposition.

1.11.1. Co-Precipitation method

The term co-precipitation describes the process of loading one or more types of material upper precipitate by the nucleation and grain growth [47]. This method is a widely used for iron oxide nanoparticles synthesis due to available, Abundance of precursor materials that are non-toxic, fast and easy. So, it plays an effective role in biomedical applications. The disadvantages of this method include the pollution of the produced precipitation with species of precursor, produced an irregular morphology [48, 49] The synthesis process involves mixing iron salts (such as sulfates, chlorides, and nitrates) with a base solution (such as NaOH) and dissolving them in an aqueous solution in an inert nitrogen atmosphere at room temperature. This leads to precipitation of iron ions (II, III) in the aqueous solution. Finally, the nanoparticles are dried to

remove solvents and iron hydroxides. Using this method, nanoparticles can be obtained with a diameter value lower 40 nm and high productivity. The temperature, type of salts, and acidic function are important factors that determine the shape, size and magnetic properties of the prepared iron oxide nanoparticles. The synthesis route by co-precipitation consists of two steps: the first step is rapid nucleation until the concentrations of the used substances reach the supercritical saturation. The second step is depended on the diffusion of dissolved species on the surface of the crystalline material that leads to the slow growth of the nucleus [50]. This method used to preparation Fe_3O_4 with and without surfactants.

1.11.2. Sol–Gel Technique

One of the methods of wet chemical synthesis includes two steps, the first step is the hydrolysis and condensation of metal alkoxides (precursors) to lead to the dispersion of the alkoxides in the solution. The second step is the drying process of the gel solution via removing the solvents or via a chemical reaction to produce a metal oxide network. Water is used as a solvent, while the precursors are dissolved in water with the help of a base or acid. The nature of precursors, acidic function, temperature, and ionic strength are influencing factors that determine the required structure of the prepared iron oxide nanoparticles [51]. Due to the fact that iron oxides have a high surface energy, they cause nanoparticles agglomerate, and this leads to increased particle size. To overcome of nanoparticle agglomeration during the synthesis process, modifying its surface by coating them with organic or inorganic molecules. The advantages of the sol-gel method are being simple, less expensive, good particle size control, homogeneous crystals, monodispersed, and high stability in aqueous solution [52].

1.11.3. Hydrothermal Technique

One of the wet chemical processes for the high-pressure, high-temperature synthesis of metals and metal oxides. The method includes the use of Teflon-lined stainless-steel autoclave at high pressure up to 200psi and high temperature up to 200°C in aqueous medium. Supersaturation of the medium occurs when low solubility of oxides or mineral salts is dried in aqueous solution. The advantages of the hydrothermal method include the possibility of controlling particle size, high crystallinity, generation of unique condensed phases, and high efficiency of the materials used [53]. Ferric sulfate, ferric nitrate, and ferrous chloride are used to synthesize hematite iron oxide nanoparticles.

In contrast, ferric ammonium citrate is used to synthesize magnetite nanoparticles. The process of synthesis of magnetite includes the use of CO as a reducing agent resulting from the decomposition of ammonium citrate at a high temperature to reduce the Fe^{3+} to Fe^{+2} . Because of the ability of carbon monoxide to miscible in a supercritical aqueous solution of grant the autoclave completes reduction of all the reactants in order to continue the reaction under supercritical conditions [54]. Synthesized hematite nanoparticles using ferric ammonium sulfate and ferric nitrate in a high-temperature autoclave within a time 5-30 seconds. The nucleation and grain growth processes can control particle size during crystallization. Temperature also plays an effective role in the nucleation process due to its ability to reduce size and increase the grain rate at higher temperatures. Also, the precursor concentration and the residence time effect on the particle size and morphology, both of observed to increase the particle size while the residence time was a stronger effect than the concentration. The hydrothermal method was able to synthesize

compounds in different shapes are nanospheres, nanosheets, nanoplates, nanorods, nano cubes, nanorings, nanowires, etc. [55].

1.11.4. Thermal Decomposition

A method frequently used to create high-crystalline iron oxide nanoparticles. The method involves continuous heating of a mixture of non-magnetic organometallic salts, solvents and surfactants in an oxygen-free atmosphere with a temperature sufficient for chemical dissociation. Then the nanoparticles grow and agglomerate. Argon gas is used because it can maintain the atmosphere inert for a longer period. Correspondingly, the dissociation temperature is in the range (100-350)°C. It uses non-magnetic materials such as ferric (III) acetylacetonate and iron carbonyls, and surfactants such as fatty acids. Finally, it is possible to produce iron oxide nanoparticles with a high level of uniformity and an average size of 10-30 nm. Changing the reaction duration and dissociation temperature can also affect particle size [56].

1.12. Eosin Yellow Dye

Eosin belongs to a group of fluorescent red dyes (an acidic dye). It is a synthetic fluorescein derivative that is made up of the molecules eosin Y and eosin B. Much more frequently, eosin Y is employed. It is a fluorescein tetrabromo derivative with a light-yellow hue. You can further differentiate eosin Y into water-soluble and ethanol-soluble varieties. According to the researcher's observations, ethanol-soluble eosin Y pollution more quickly and produces a more vividly red color than water-soluble eosin Y. Eosin B, a dibromo dinitro derivative of fluorescein, with a tinge of blue. The performance of eosin B is on par with that of eosin Y, and it occasionally produces a brighter red hue. Eosin can be used to stain muscle fibers, collagen, red blood cells, and cytoplasm [57, 58]. Eosin Y

is frequently utilized in biological tissues as a counterstain. The most used method for staining histology material is hematoxylin-eosin. In addition to their, it use as coloring agent in textiles, food, cosmetics, pharmaceuticals and are increasingly being used in the manufacture of ink. In actuality, all traditional red inks are diluted eosin solutions. The enormous requirement for dyes in the industrial sector has led to the introduction of these toxic, poorly biodegradable dye molecules into our ecosystem; as a result, become immediate and effective remediation is necessary[59].

Table (1.3): Properties of eosin yellow dye [60, 61].

Property	Value
Conventional name	Eosin yellow
Various names	Eosin dye, bromoeosine, tetrabromofluorescein.
Molecular Formula	$C_{20}H_8Br_4NaO_5^+$
Molecular Weight	670.9 (g/mol)
Maximum wavelength	518 nm
Class	xanthene dye
Ionization	Acid
Color	Yellow
Solubility, aqueous	40%
Solubility in ethanol	2%

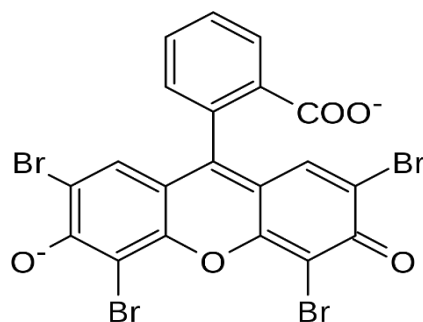


Figure (1.5): Structure of the eosin yellow dye[61]

1.13. Literature Survey

Shideh et al. [62] (2012) synthesized of Magnetite (Fe_3O_4) nanocrystals using facile hydrothermal method. It was discovered that as the hydrothermal temperature rose from 100 °C to 200°C, the average crystallite size and physical size of the generated nanocrystals also increased. The resulting Fe_3O_4 nanocrystals exhibit superparamagnetic behavior, and when the hydrothermal temperature rises.

Hernandez et al. [63] (2015) prepared Fe_3O_4 nanoparticles via the thermal decomposition method and employed as surface to remove methylene blue dye from contamination solutions. The presence of a structural Fe_3O_4 phase, in which the granules have an acicular shape, was confirmed by X-ray diffraction. These nanoparticles display superparamagnetic properties, as evidenced by the hysteresis loops produced by a vibrating sample magnetometer.

According to **Cherukutty et al.** [64] (2018), employed the solvothermal method to prepare Fe_3O_4 NPs and $\text{Fe}_3\text{O}_4/\text{rGO}$ nanocomposites as adsorbents for the removal of the methyl violet (MV) dye. The greatest adsorption capacity for FG2 was measured at 196 mg/g. For FG1 and FG2, the adsorption isotherms and kinetics suit the Langmuir and pseudo-second-order kinetic model more accurately. Reduced dye adsorption sites are caused by increased Fe_3O_4 loading on

rGO, and magnetic separation is impacted by too little Fe_3O_4 loading. For the adsorption process and quick separation of the adsorbent, the ideal Fe_3O_4 loading on rGO is a crucial parameter.

Rahmawati et al. [65] (2019) prepared magnetite (Fe_3O_4) nanoparticles by both coprecipitation and co-precipitation-ultrasonic irradiation methods. This study showed that ultrasonic irradiation could lessen the accumulation that takes place during the synthesis process, resulting in particles with a clear, nearly homogenous shape.

Xiaoduo et al. [66] (2019) prepared of Fe_3O_4 nanoparticles by sol-gel assisted method and annealed under vacuum at different temperature 200-400°C, used Fe_3O_4 nanoparticles functionalized activated carbon as efficient surface to removing rhodamine B (RhB) and methyl orange (MO) from solution. It was found that an adsorbate quantity of the prepared surface towards rhodamine and methyl dye are 182.48 mg. g^{-1} and 150.35 mg. g^{-1} , respectively. An exothermic and spontaneous adsorption process was discovered when the thermodynamic parameter was further studied. This composite has a high rate of magnetic separation and adsorption, has the potential to be a valuable and recyclable adsorbent for processes for treating and purifying wastewater.

Zakiyyu et al. [67] (2019) reported the preparation of Fe_3O_4 nanoparticles using a sol-gel and annealed them under vacuum at various temperatures ranging from 200 °C to 400 °C. The Fe_3O_4 nanoparticles were successfully characterized in their phase and molecular structure, functional group, morphologies, and roughness analyses; the findings showed that different-sized Fe_3O_4 nanoparticles were produced. The fabrication of Fe_3O_4 nanoparticles using this process offers a number of important advantages. First off, the synthetic approach uses less expensive, hazardous free iron salts, making it economically significant and environmentally beneficial. Second, by adjusting the annealing

temperature, the size of the produced Fe_3O_4 nanoparticles may be easily regulated.

Joshi et al. [68] (2019) prepared $\text{Fe}_3\text{O}_4@$ activated carbon nanoparticles were by co-precipitation methods. Different techniques were used to characterize the $\text{Fe}_3\text{O}_4@$ AC nanoparticles, and the results showed that the synthesized nanoparticles had a diameter of 6-16 nm. For the dyes methylene blue and brilliant green, the absorption capacities of $\text{Fe}_3\text{O}_4@$ AC were determined to be 138 mg/g and 166.6 mg/g, respectively.

Venkatesha et al. [69] (2021) synthesized graphene oxide based magnetic nanocomposite using the coprecipitation method. The ability of magnetic nanocomposite to adsorb industrial dyes Methylene Blue and Rhodamine Blue is put to the test. The dye concentration, adsorbent dosage, and adsorption time are all optimized in the dye removal tests (0.1 g/L graphene oxide, 10 mg/L of dyes, and a 25 min adsorption time). For MB and RB, adsorption capacities of 100 and 80 mg/g, respectively, were attained.

Beata et al. [70] (2021) prepared ferrimagnetic magnetite (Fe_3O_4) nanoparticles using Massart's method. Then, done of functionalized form (f-MNPs) with succinic acid, L-arginine, oxalic acid, citric acid, and glutamic acid. According to the study results of the XPS analysis of the elements and their chemical states on the surfaces of MNPs and f-MNPs, there are variations in the types of iron oxide, the number of carbon-oxygen groups, the chemical bonds between the atoms, the magnetic properties, and the molecules that are adsorbed. The biocompatible surfaces for L929 cells demonstrated variable cytotoxicity for HeLa cells (10.8-5.3% of cell death), with MNPs functionalized with oxalic acid having the highest cytotoxicity.

1.14. Aim of the study

The aims of this project are to:

- A.** Prepare of magnetic Iron oxide (Fe_3O_4) nanostructure as a catalyst.
- B.** Study the effect of using positive, negative and neutral surfactants on the preparation methods.
- C.** Study the properties of the as-prepared nanostructure using Inferred spectroscopy (FTIR), X-ray diffraction (XRD), Scanning electron microscopy (SEM).
- D.** Study the adsorption of the eosin yellow dye in a liquid – solid system.
- E.** Study the different parameters on removal process of dye such as effect of catalyst (iron oxide), equilibrium time, masses, initial pH, and temperature.
- F.** Study of sorption isotherm models and thermodynamic functions.

Chapter Two: Experimental Part

Chapter Two Experimental part

2.1 Chemicals and Instruments

2.1.1. Chemicals

The chemicals and reagents used in this study are listed in Table (2-1).

Table (2.1): Chemicals and Reagents

Materials	Formula	Company supplied	Purity and percentage %
Absolute ethanol	C_2H_5OH	Carlo erba, France	99.9
Cetrimide (CT)	$C_{17}H_{38}BrN$	CDH, India	99
Cetrimonium bromide (CTAB)	$CH_3(CH_2)_{15}N(Br)(CH_3)_3$	CDH, India,	99
Eosin yellow dye	$C_{20}H_6Br_4Na_2O_5$		99
Hydrochloric Acid	HCl	BDH company, England	(35)%
Iron (II)sulphate heptahydrate	$FeSO_4 \cdot 7H_2O$	BDH company, England,	99.98
Sodium dodecyl sulfate (SDS)	$CH_3(CH_2)_{11}OSO_3Na$	CDH, India	90
Sodium hydroxide	NaOH	BDH company, England	99.99
Sodium nitrate	$NaNO_3$	BDH company, England	99
Triton (X100)	$t\text{-Oct-C}_6\text{H}_4\text{-}$ $(OCH_2CH_2)_xOH, x= 9\text{-}$ 10	CDH, India	99

2.1.2. Instruments

Table (2.2) describes the employed instruments in this study with their companies and places.

Table (2.2): Employed instruments.

Instruments	Companies	Places
Double -beam-UV-Visible spectrophotometer	AA-1800, Shimadzu, Japan.	University of Kerbala, Science college .
Digital pH meter	OAICTON-2100, Singapore	University of Kerbala, Science college
Electrical hot plate	Heido-MrHei-Standard, Germany	University of Kerbala, Science college
FT-IR Spectrometers	Shimadzu,8400S Japan	University of Kerbala, Science college
Oven	Memmert, Germany.	University of Kerbala, Science college
Scanning Electron Microscopy (SEM)	(kyky EM) 320., USA.	Isfahan University, Iranian Islamic Republic
Sensitive balance	BL 210 S, SartoriusGerman	University of Kerbala, Science college
Shaker machine	Lab companion	University of Kerbala, Science college
X-Ray Diffraction Spectroscopy	Lab X- XRD 6000, Shimadzu, Japan	Isfahan University, Iranian Islamic Republic

2.2. Preparation of Standard Solutions**2.2.1. Preparation of Eosin yellow dye Solution**

A stock solution of Eosin yellow dye (100 mg/L) was prepared by dissolving (0.1 g) in (1000 mL) distilled water. Then dilute solutions of this dye were prepared with concentrations ranging from (1 to 50) mg/L through the process of dilution with distilled water.

2.2.2. Preparation of Acid Solution

25 mL of hydrochloric acid solution was prepared at a concentration of 3 mol/L, as 6.62 mL of concentrated hydrochloric acid (1.18 g/mL, 35 % and 36.46 g/mol) was added to a volumetric bottle of 25 mL containing half of distilled water, then the process was completed by adding water. Carefully cold distilled to the vial to the mark until obtained a volume of 25 mL.

2.2.3. Preparation of $\text{FeSO}_4 \cdot 7\text{H}_2\text{O}$ Solution

250 mL of Ferric sulfate was prepared at a concentration of 0.033 mol/L with a molecular weight of 278 g/mol by dissolving 3.33 g of $\text{FeSO}_4 \cdot 7\text{H}_2\text{O}$ in a 250 mL volumetric flask and then completing the solution with distilled water to the mark to get 250 ml of $\text{FeSO}_4 \cdot 7\text{H}_2\text{O}$.

2.2.4. Preparation of NaOH Solution

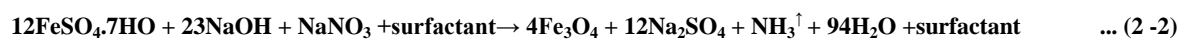
1 M of sodium hydroxide was prepared by dissolving 2 g of NaOH in a 50 volumetric vial and then completing the solution with distilled water to the mark.

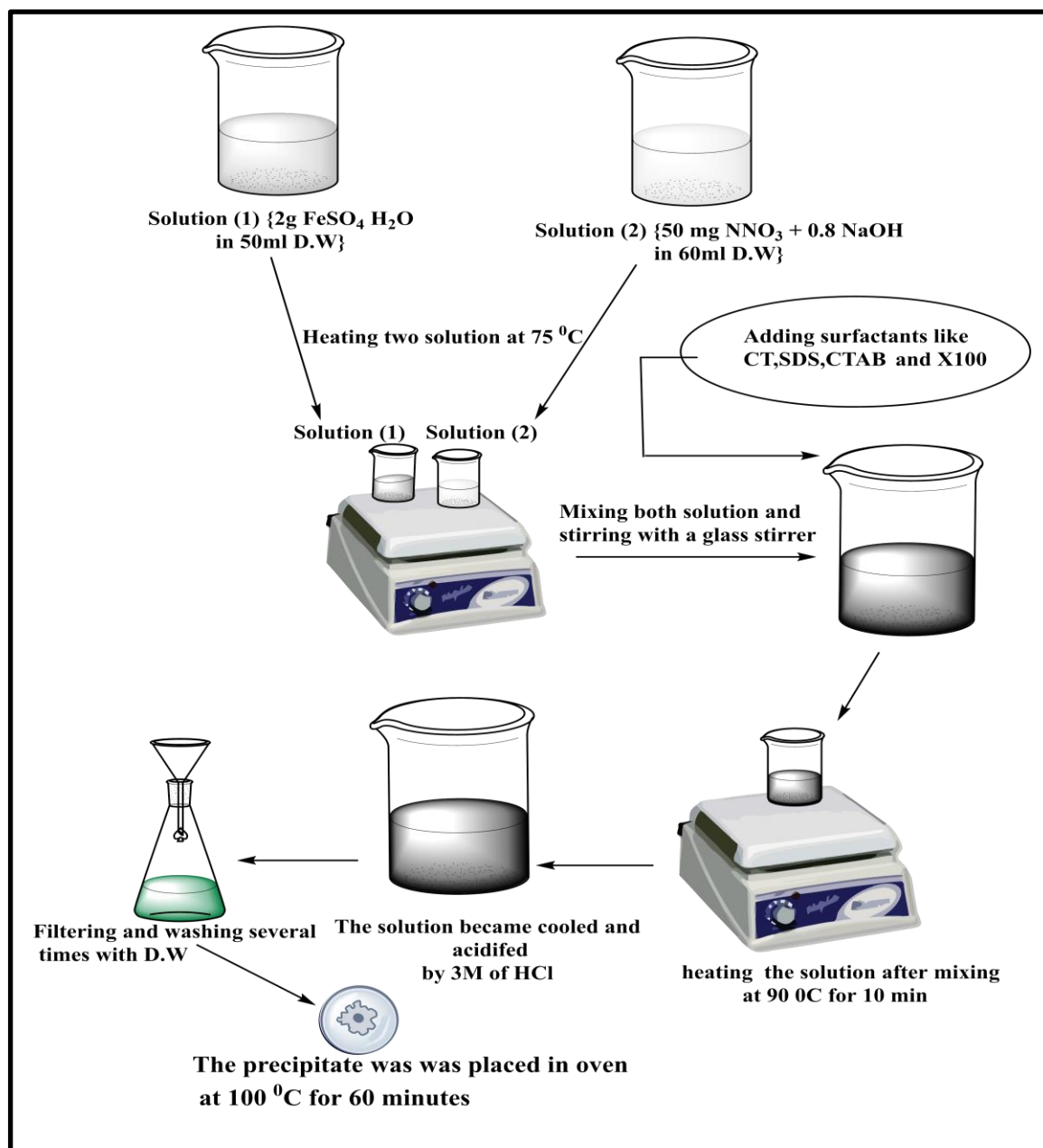
2.3. Preparation of Iron Oxide Nanoparticles**2.3.1. Synthesis of Spinel Fe₃O₄ nanoparticles without Surfactant**

150 mL of FeSO₄·7H₂O of 0.033 mol/L was put in a 400 mL beaker. (50 mg of NaNO₃ and 0.56 g of NaOH) were dissolved in 60 mL of distill water then put in a 100 mL beaker. Both solutions were heated to 75 °C and mixed together using the glass rod then heated to 90 °C for 10 minutes. A tong was used to pick up the produced hot solution. A green suspension was created, which quickly turned black. The black color suspension was cooled to 20 °C. A Buchner funnel was used to filter this black suspension. The resulting black precipitation was washed twice with 50 mL of water to remove all salts, and then dried in a 100 °C oven for 60 minutes. Figure (2-1) shows how the black powder was scraped off the filter paper.

2.3.2. Synthesis of Spinel Fe₃O₄ nanoparticles with surfactants

The same measures were taken as mentioned in the previous paragraph (2.4.1) and adding surfactants such as (positive surfactant (CT (cetramide) CTAB and, negative surfactant (SDS), and neutral surfactant (X-100) after both solutions were heated to 75 °C and mixing the both solutions, then completing the other steps in this paragraph (2.4.1) as shown in Figure 2-1. The chemical reactions of spinel Fe₃O₄ without and with surfactant were proposed using the equations below.





Scheme (2-1): The schematic diagram of the steps of Spinal Fe_3O_4 Nanoparticle Preparation.

2.4. Characterization of Spinal Fe_3O_4

2.4.1. FT-IR Spectroscopy

The FT-IR spectra of the Fe_3O_4 with and without surfactant substance were obtained using CsI powder in the range $(400-4000) \text{ cm}^{-1}$ using (FT-IR Spectroscopy, Shimadzu).

2.4.2. X-Ray Diffraction Spectroscopy (XRD)

Scherer's equation (eq.3) was used to calculate the mean Crystal sizes (L) of all samples,. The equation was based on X-Ray data Diffraction (XRD). Shimadzu's Lab. XRD 6000 instrument was used to analyze the XRD data. This instrument employs magnetite with and without surfactant substance as a target source with a wavelength of (0.15406 nm), a voltage of 40.0 kV, a current of 30 mA, a speed of 12.0000 (deg/min), and an angle (2) range of (20 - 80) deg.

$$L = \frac{k\lambda}{\beta \cos \theta} \quad \dots(2-3)$$

Here: θ = Bragg angle, λ = 0.15406 nm = wave length of X-ray, $\beta_{1/2}$ =Full Width Half- maxima (FWHM), (D or L) = crystallite size of particle. and k = the Scherer constant with value from (0.84 to 0.94) [71, 72].

2.4.3. Scanning Electron Microscopy (SEM)

SEM analysis (FESEM FEI Nova Nano SEM 450) was used to measure the scanning electron microscopy image for all samples (Fe_3O_4 with and without surfactant substance).

2.5. Factors Influencing on the Removal the Dye**2.5.1. Equilibrium Time**

In order to know and determine the time required to achieve equilibrium between the adsorbent surface and the adsorbent, volumetric bottles with a capacity of 25 mL were used, in which a concentration of 10 mg/L and a surface weigh of 0.01g was used for the dye in (60) min. and temperature 298 K, the solutions were separated using magnets, and then the absorbance was measured at the maximum wavelength 516 nm.

2.5.2. Effect of the Weight of Surface Adsorbent

Changing the weight of the adsorbent surface has an effect on adsorption, so it was studied using concentrations of 10 mg/L of dye and by using different weights of the adsorbent surfaces ranged between (0.005, 0.01, 0.02 and 0.03) g for magnetite then using a shaking time of (60) min. With the laboratory temperature set at about (298)K. After that, these solutions were separated using a magnet, and the absorption at the greatest wavelength of the dye was measured using a UV-visible device, then the concentration of each dye at equilibrium (C_e mg/L) was found based on curves. The previous prepared titration was then calculated as the percentage of removal.

2.5.3. Effect of pH on the dye

The effect of changing the acidity function on the removal rate and the adsorption process was studied by using concentrations of 10 mg/L of dye, while fixing the best conditions for the adsorption process, with the change of the acidic function within the range (pH = 3,5,6.5,9 and 12), after that. The same measures were taken as mentioned in the previous paragraph (2.6.2).

2.5.4. Effect of Temperature

The temperature has an effect on the adsorption process, so it was studied and the adsorption capacity was known using concentrations of 10 mg/L for the dye with fixation of the best conditions for the removal process, with changing temperatures within the temperature range (278 - 323) K. Using magnetite as an adsorbent. The identical steps as those indicated in the previous paragraph were taken (2.6.2).

2.6. Adsorption Isotherm

In order to obtain the adsorption isotherm for the dye with the adsorbent surface (magnetite), different concentrations were used that ranged between (5,10,15,20 and 25) mg/L of the dye with a weight of 0.01 g of magnetite, with an adjustment of the acidity function. Within the limits of (pH= 6.7) using a shaking time of (10 to 60) min, and temperature 298 K. The solutions were separated using magnets, and then the absorbance was measured at the maximum wavelength 516 nm. as shown in the following equation[73]

$$A = m C_e + b \quad \dots\dots\dots(2-4)$$

A = absorption, m = Slope, C_e = equilibrium concentration (mg/L), b = Intercept.

After determining the C_e values, the values of the adsorption weight capacity (Q_e) were extracted from the following equation [74]

$$Q_e = \frac{V(C_o - C_e)}{m} \quad \dots\dots\dots(2-5)$$

Where Q_e = weight adsorption capacity in units of (mg/g), C_e = the equilibrium concentration of the adsorbent solution in units of (mg/L), C_o = the initial concentration of the adsorbent solution in units of (mg/L), V = total volume of the adsorbent solution in units (L), m is weight of the adsorbent in units of (g).

The percentage of dye removal (E%) was also calculated using the following equation (2-5) [75].

$$E \% = \frac{C_o - C_e}{C_o} \times 100\% \quad \dots\dots\dots(2-6)$$

2.7. Equilibrium Isotherm Modeling

By adding 0.01g Fe_3O_4 to various dye concentrations (from 5 to 25) mg/L and temperatures (from 5 to 30) °C with the proper pH adjustment, decolonization isotherms were discovered. The ideal isotherm model was described using

experimental data at equilibrium amounts of dye adsorbed (q_e) on the adsorbent (Fe-oxide) and dye concentration in solution (C_e) at constant temperatures and pH levels. The equilibrium data were described by linear versions of the Langmuir and Freundlich equations (Table 2.3). Correlation coefficients were used to compare how applicable these equations were (R^2) [73].

Table (2.3): Different isotherm models used in this study and their linear forms

Isotherm	Nonlinear form	Linear form	Plot
Langmuir	$q_e = \frac{KLCe}{1+KLCe}$	$\frac{1}{q_e} = \left(\frac{1}{Kl\ qm}\right) 1/Ce + \left(\frac{1}{qm}\right)$	$\frac{1}{q_e}$ VS $\frac{1}{C_e}$
Freundlich	$q_e = K_F C_e^{1/n}$	$\text{Log } q_e = \text{log } K_F + 1/n \text{ log } C_e$	$\text{Log } q_e$ VS $\text{log } C_e$
Temkin	$q_e = \frac{RT}{bT} \ln(KT C_e)$	$q_e = \frac{RT}{bT} \ln KT + \frac{RT}{bT} \ln C_e$	q_e vs. $\ln C_e$

Chapter Three:

Results and Discussion

Chapter Three Results and Discussion

3.1. Verify the Elements of the Preparation Equation Fe_3O_4 NP

Preparation of Fe_3O_4 NP in the presence and absence of surfactant according to the method described in paragraph (2.4) and the results of equations (2-1 and 2-2) were inferred by conducting a number of detections that showed the formation of sodium sulfate, it was in a soluble state in the filtration solution. It was noticed that the addition of barium chloride to the filtrate was white turbidity due to barium sulfate as explained in the Fig 3.1(a). As for ammonia in a gaseous state where a white cloud is formed on the rod glass moistened with HCl near the beaker's nozzle, and the color of the litmus paper changed from red to blue as shown in the Fig 3.1(b) and this indicates that the formed precipitate is only magnetic iron. It was inferred by the attraction of magnet

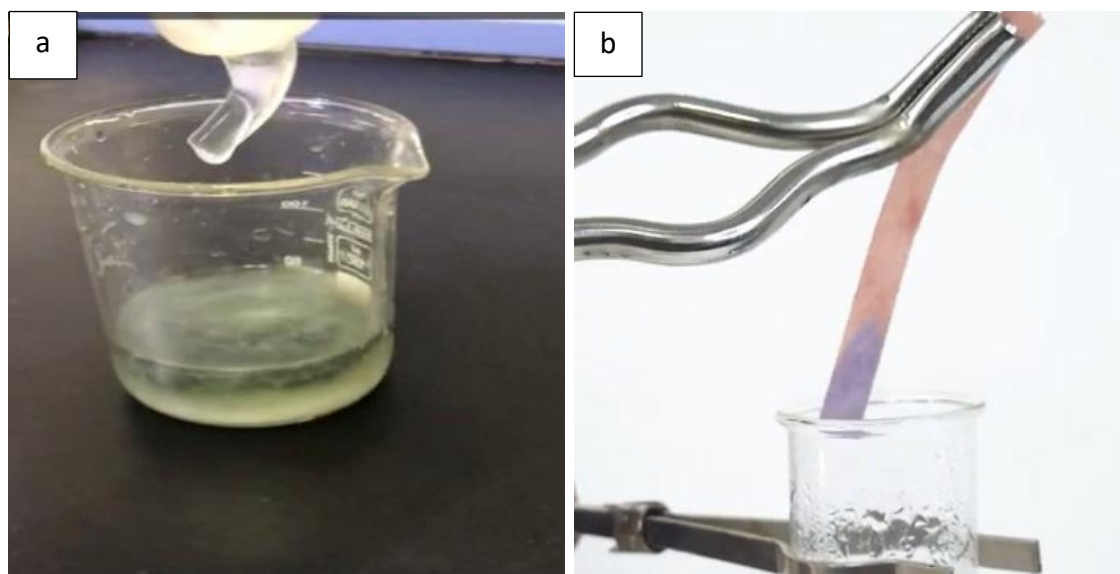


Figure (3.1): Detection of the Chemicals Compounds During the Magnetic Iron Nanoparticle Preparation such as (a) Na_2SO_4 solution and (b) NH_3 gas.

3.2. Characterization of Fe-oxide NPS

FT-IR, X-Ray Diffraction (XRD), scanning electron microscopy (SEM) and Energy-dispersive X-ray spectroscopy (EDX) were used to evaluate the generated Fe₃O₄ nano powder. The details regarding chemical composition were given by EDX. By using SEM, the oxides' shape and particle size were evaluated. The information regarding the crystalline structure and particle size was discovered using XRD analysis.

3.2.1. FT-IR spectral analysis

The identification of substances is helped in some qualitative ways by FT-IR spectrum analysis. IR light is absorbed by both inorganic and organic substrates, making them IR active. Oxides and hydroxides of metal nanoparticles typically produce an absorption peak below the wavelength of 1000 nm, or in the finger print zone, as a result of interatomic vibrations. FT-IR spectra of Fe₃O₄ with and without surfactants are shown in Figure 3.2 to provide some insight into the structure of the synthetic oxides. Figure a the large peak at 3163.36 cm⁻¹, which belongs to the O-H group, as well as the peak at 1100 cm⁻¹, which explains the O-Fe-O as an octahedron bending, are both seen in the FTIR spectra for all manufactured magnets. Form b depicts the broad peak at 3340 cm⁻¹ beyond to the O-H stretching of the iron oxide and another peak at 3028 cm⁻¹ assignment to the N-H bending in addition to the peaks between 2924 and 2850 cm⁻¹ represent stretching C-H. As for the Fe-O bonding, it is in locations between 640 and 598 cm⁻¹ that present to the tetrahedral curvature [76, 77]. The O-H bending is explained by the peak at 1207 cm⁻¹. Fe-O octahedral and tetrahedral bending are shown by the more intense bands between 744 and 598 cm⁻¹[78]. The same is true for the spectra of c, d, and e; the magnetic iron oxide spectrum shows the same peaks, with the addition of a few different peaks that are associated with the active groups in the surfactant molecule.

The same holds true for the spectra of c, d, and e, with the addition of some distinct peaks that are related to the functional groups in the surfactant molecule, such as the peak at 3159 cm^{-1} that denotes N-H bending, the peak at 1111 cm^{-1} that illustrates O-Fe-O the octahedron bending, and the absorption at 1739 cm^{-1} that was brought on by C=O stretching in Figure (e).

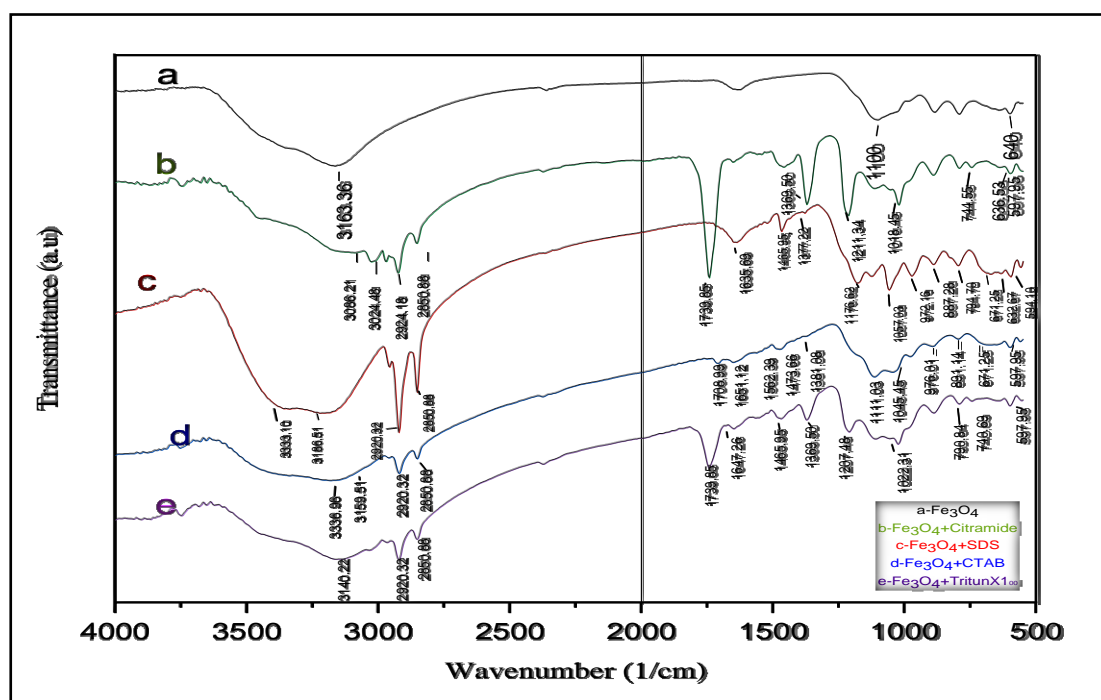


Figure (3.2): The FT-IR spectra of magnetite with and without surfactants, including Fe_3O_4 (a), Fe_3O_4 +CT (b), Fe_3O_4 +CTAB (c), Fe_3O_4 +SDS (d), and Fe_3O_4 +Triton X100 (e).

3.2.2. X-ray diffraction (XRD) analysis

The crystallographic structure, chemical makeup, and physical characteristics of materials can all be learned about using the non-destructive analytical technique known as X-ray scattering. This method is based on measuring the intensity of an X-ray beam that scatters when it hits a sample as a function of incident and scattered angles, polarization, and wavelength or energy. Based on the elastic scattering of X-rays from the individual atoms' electron clouds, X-ray diffraction provides information about the atomic structure of materials. The

dynamical theory of diffraction provides the most thorough explanation of crystal scattering. In polycrystalline or powdered solid materials, powder diffraction (XRD) is a technique used to characterize the crystallographic structure, crystallite size (grain size), and preferred orientation. By comparing diffraction data to a database kept by the International Centre for Diffraction Data, powder diffraction is frequently used to identify unidentified compounds. Magnetite NPS with and without surfactants, XRD patterns are shown in Fig. 3.3. The scattering pattern for the tested samples powder, 2θ at $\lambda = 1.54056$ nm as a function of Bragg angle is shown in those figures. Figure (3.3-a) shows the results of an XRD analysis of magnetic iron oxide nanoparticles made without the use of surfactants. Diffraction peaks' occurrence at 2θ values of 18.96° (111), 30.4° (220), 35.64° (311), 43.4° (400), 53.16° degrees (422), 57.32° degrees (511), 63.12° degrees (440), and 73.12° degrees (553) are in agreement with the common XRD results of the spinel Fe_3O_4 structure. Additionally, it was noted that when surfactants were applied, some values vanished and their relative intensities varied, with the peak at 2θ values of 18.96 degrees (111) disappeared when using Triton X100, Cetrimide, and CTAB in addition to the increase in the relative strength of the 35.64° degrees peaks. (311), 43.4° degrees (400), 53.16° Degrees (422), 57.32° degrees (511), 63.12° degrees (440), and 73.12° degrees (553). When both ceramide and CTAB are used, the prepared nanoparticles. The position and relative strength of the diffraction peaks agree well with the standard phase magnetite NPs diffraction pattern of the International Center of Diffraction Data card. The Fe_3O_4 nanoparticles for all forms in figure 3 (a) to (e) are well crystalline (JCPDS No. 19-0629)[79]. Using the Debye-Scherrer formula according to the equation (2-3), the mean crystal diameters of the produced magnetite nanoparticles without and with surfactants were computed [71, 72]. Due to its size value being less than 10 nm, iron oxide nanoparticles were considered to have a quantum dot, with a mean crystal size of 8.5 nm. This value is consistent with other nanoparticle studies that have been described in references [80, 81]. However, the mean crystal size rises to

21.55 nm, 27.72 nm, 27.66 nm and 22.53 nm for Fe_3O_4 +Triton X-100, Fe_3O_4 +CTAB, Fe_3O_4 + SDS and Fe_3O_4 + Cetramide respectively when addition the surfactants. following the addition of surfactants during the synthesis of iron oxide NP because to the behavior of surfactants as template. The hydrophobic terminals of the iron oxide NP nanoparticle crystal are located around the surfactants, while the hydrophilic terminals are located far away from the solution. As a result, when the surfactants are dissolved in aqueous solutions, the mean crystal size of iron oxide increases. Additionally, because to his small size and magnetic properties, that will shield iron oxide from the agglomeration before adding the surfactant materials.

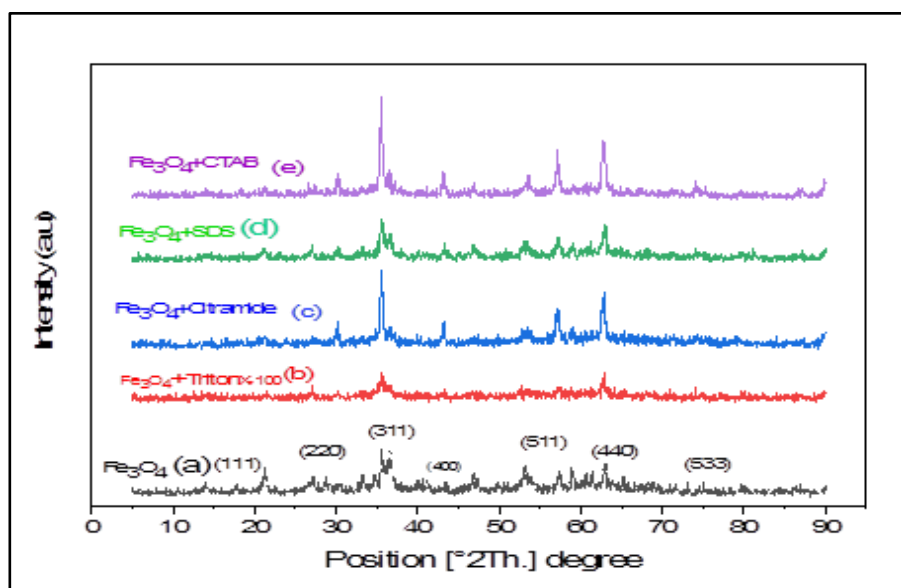
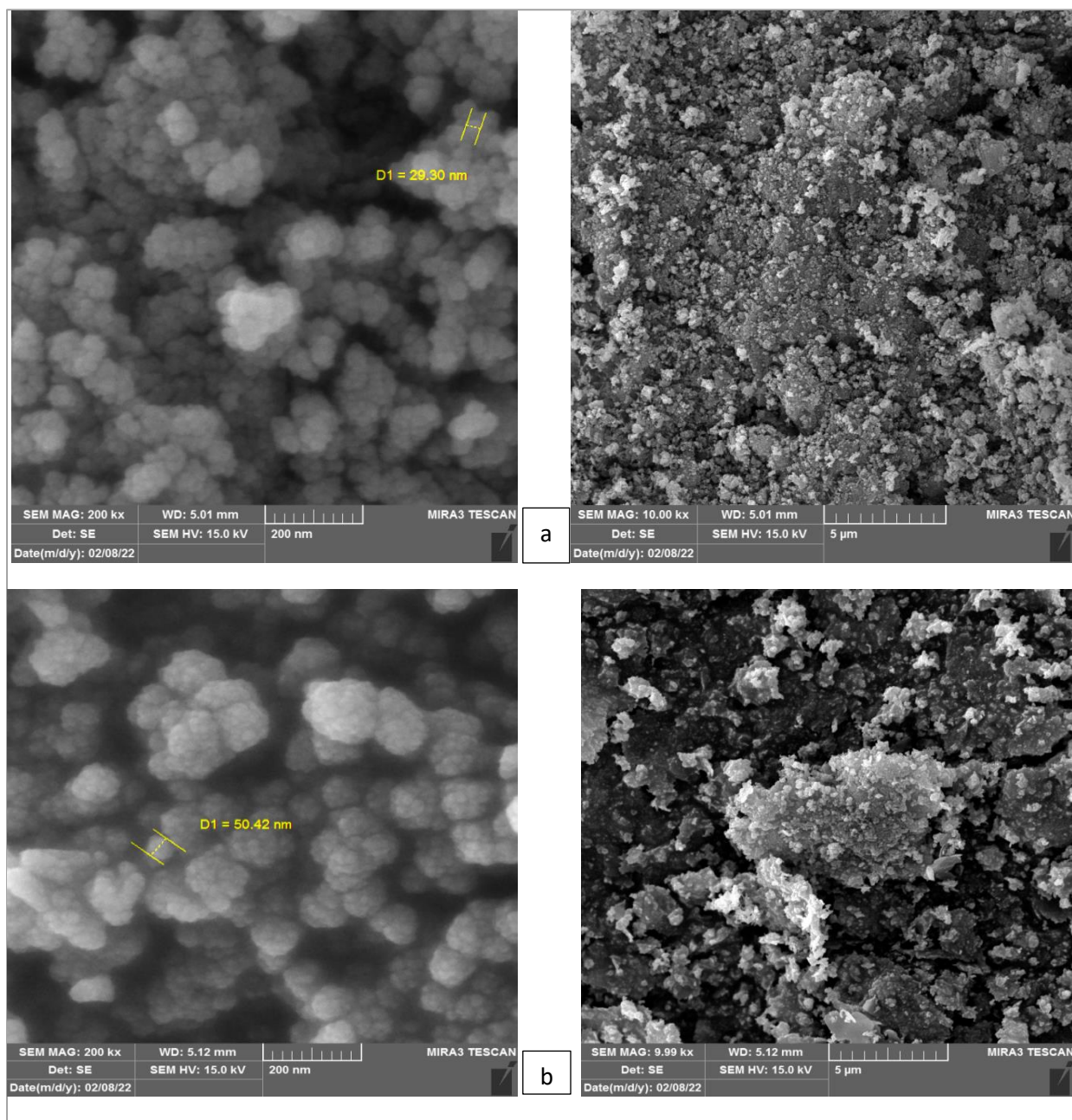


Figure (3.3): The magnetite's XRD analysis without and with its surfactants (a) Fe_3O_4 , (b) Fe_3O_4 +Triton X-100, (c) Fe_3O_4 +Cetramide, (d) Fe_3O_4 + SDS and (e) Fe_3O_4 +CTAB.

3.2.3. Scanning electron microscopy (SEM) analysis

The surface of the sample is imaged by the scanning electron microscope (SEM), a form of electron microscope, using a high-energy electron beam in a raster scan pattern. The sample is made up of atoms with which the electrons interact to produce signals that provide information about the sample's surface topography and composition. According to figure 3.4. (a-e) for the SEM study, the

small iron oxide nanoparticles are aggregated into larger particles, and the particle size of iron oxide nanoparticles was shown to grow with the following sequences: (20-30 nm), (41-50 nm), (43-52 nm), (42-50 nm), and (42-50 nm) for iron oxide NP, and with SDS, triton X100, CTAB and cetramide, respectively. This behavior indicates that all prepared NP are polycrystals, and the results are consistent with those of other studies that have been published [82, 83]



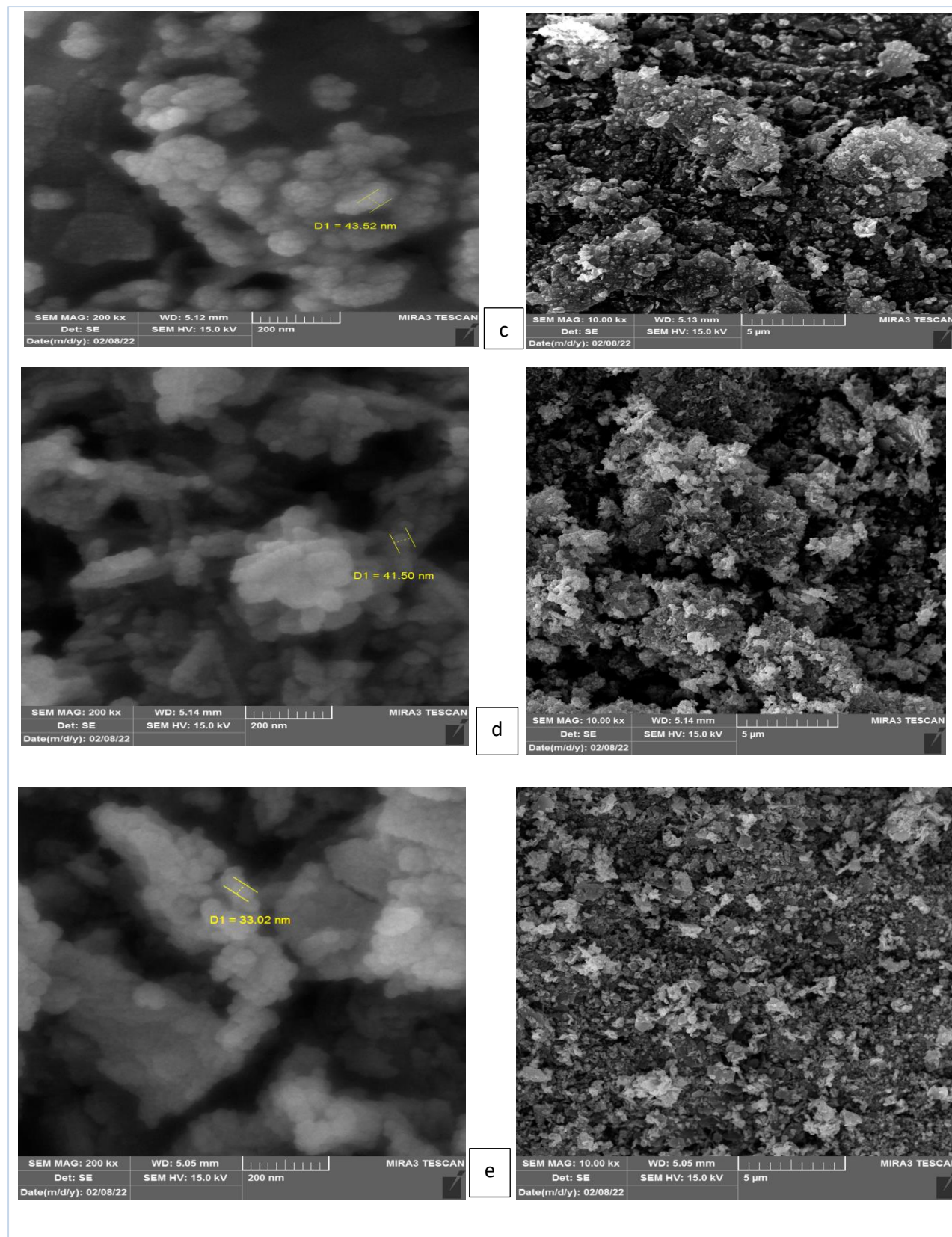


Figure (3.4): The scanning electron microscope (SEM) images of (a) magnetite without cetramide, (b) Fe_3O_4 + CT, (c) Fe_3O_4 + CTAB, (d) Fe_3O_4 + SDS and (e) Fe_3O_4 + Triton X 100.

3.3. Applying Fe₃O₄ NP in the Removal of the Organic Contaminants

The removal of contaminants represented by the Eosin yellow dye, the calculation of the dye's maximum concentration and calibration curve have both been attempted using nanomaterials, such as Fe₃O₄. The absorption spectra were recorded using a spectrophotometer (UV-visible), within the range (400-800 nm), using cells of glass thickness (1 cm), in order to identify the maximum wavelength at which the maximum absorption (λ_{max}) of aqueous solutions of Eosin yellow dye is attained. Eosin yellow dye has a value of (λ_{max}) of 516 nm, as demonstrated in Figure 3.5.

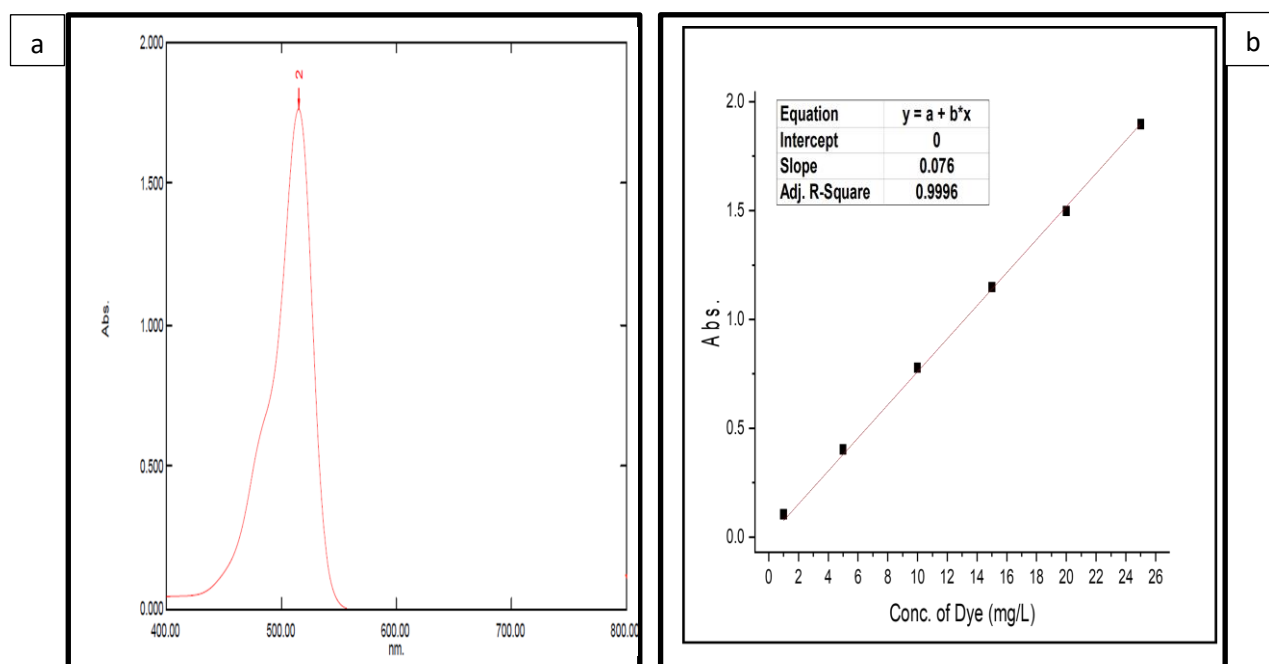


Figure (3.5): (a) UV-Visible Absorption Spectrum for an Eosin yellow dye solution (b) calibration curve for the determination of Eosin yellow dye in aqueous solution at 516 nm wavelength.

3.4. Using Magnetic Nanoparticles to Remove the Dye Eosin Yellow

The eosin yellow dye, a water contaminant, was removed using the produced nanoparticles. The % E_{removal} for utilizing Fe₃O₄ increases after using surfactants at

the varied dye concentrations of 10 and 25 mg/L, as shown in Figure 3.6. Due to the higher number of dye ion collisions with the catalyst surface (Fe_3O_4 NP) during the adsorption process, the high concentration of dye (25 mg/L) was removed more quickly than the low concentration of dye (10 mg/L). The highest $E_{\% \text{ removal}}$ achieved with (Fe_3O_4 + cetramide) as a surfactant was 94.7% at 25 mg/L dye (pale blue column) and 0.05 g of NP, and 94.6% at 10 mg/L dye and 0.05 g NP (green column).

Figure (3.6) also shows that the adsorption capacity (q_e) for employing Fe_3O_4 increases when cetramide is used as a surfactant. The greatest q_e was 2.37 mg/g when using 25 mg/L with 0.05 g of the nanoparticle (pale blue column) and 0.95 mg/g when using 10 mg/L with 0.05 g. The best results for removal are obtained when using cetramide as a positive surfactant, Figure (3.7) illustrates the role of using cetramide during the preparation of iron oxide NP.

Based on the hydrophobic part of this surfactant being arranged towards the surface of Fe_3O_4 , while the dye attractive with the hydrophilic part of surfactant that have a positive charge in aqueous solution, the attractive force will increase on iron oxide NP, which prepared in presence a cetramide. The positive charge of the surfactant will attract the negative components in the dye, enhancing the removal of the dye from aqueous solution[84, 85].

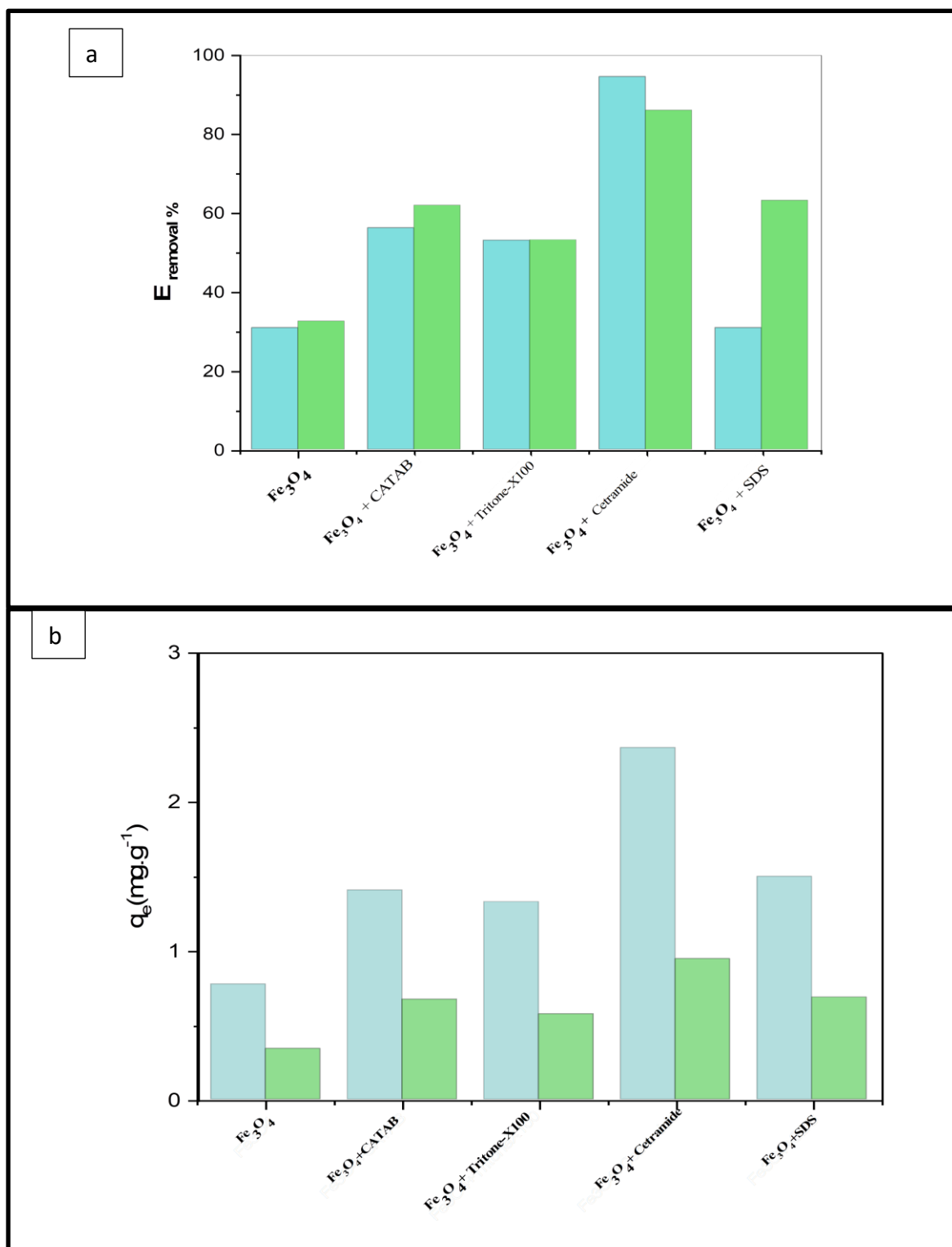


Figure (3.6): Relationship between produced nanoparticles with various surfactants and the $E_{\%}$ (a) and q_e (b) of dye removal at 60 minutes.

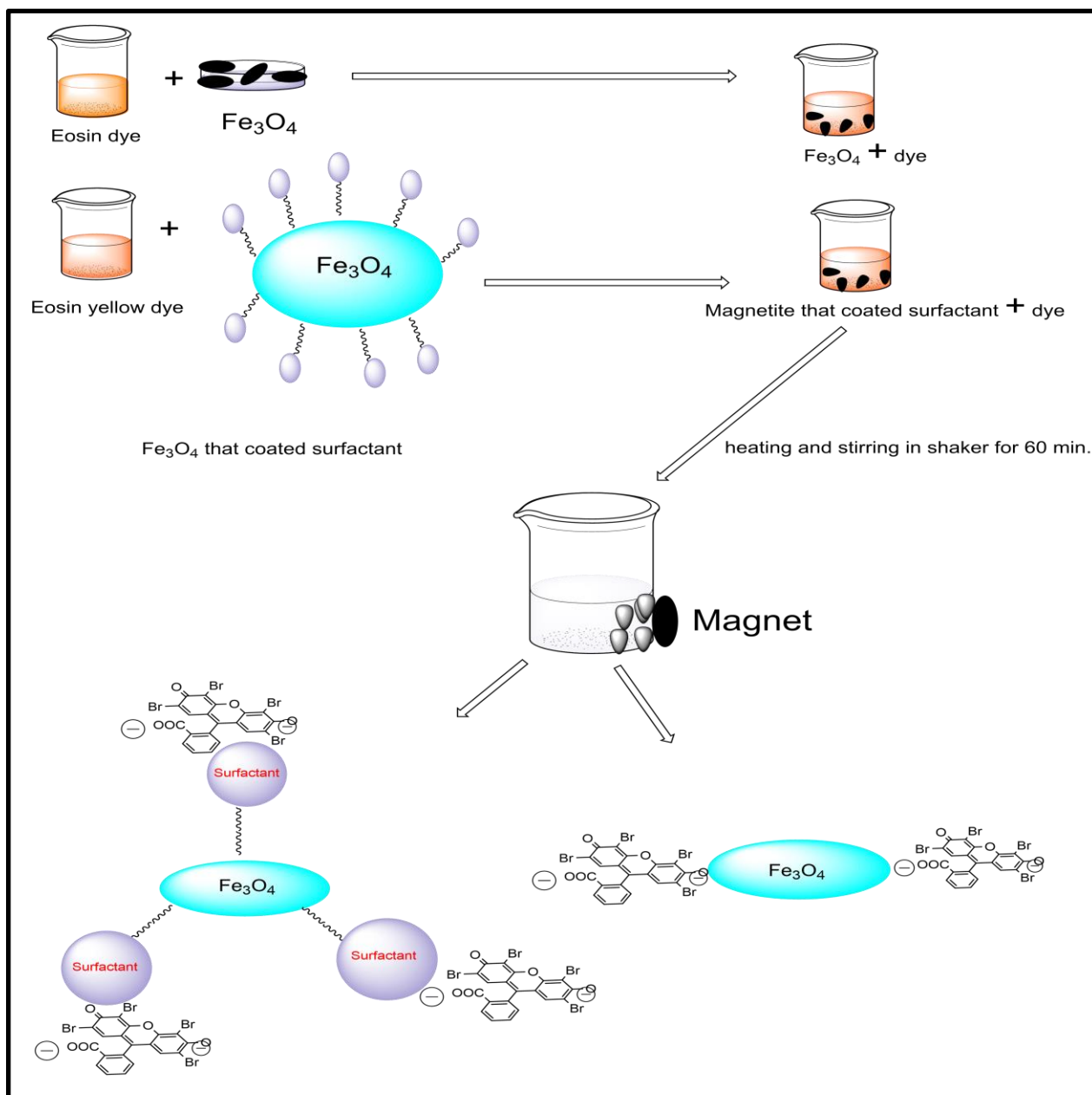
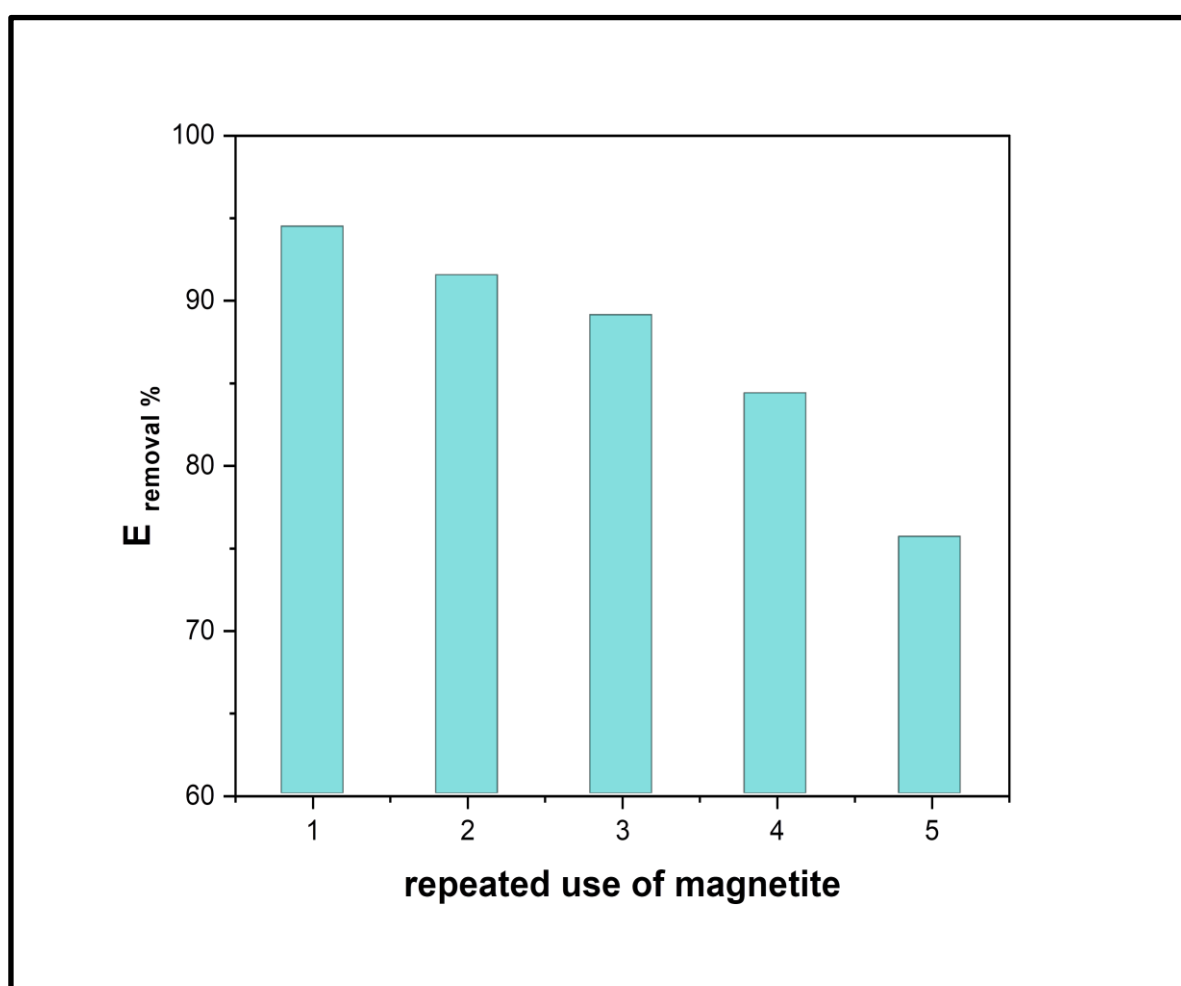


Figure (3.7): Fe_3O_4 nanoparticles in the presence of the surfactant (cetramide) are used as a mechanism to remove the dye from its solutions.

3.5. The efficiency of surfactant (cetramide) on created Fe_3O_4 nanoparticles

Due to the adsorption of eosin yellow dye (10 mg/L) by Fe_3O_4 particles created by the presence of the surfactant, this process can operate in reverse and it is the adsorption process that will diminish with repeated use at 298 K and 60 min.

This situation may arise during the saturation process of the active site of synthesized nanoparticles caused by the adsorption of dye particles. The amount of eosin yellow dye removed from aqueous solutions decreased from 94.48 % in the first stage to 75.61% Figure 3.8, which is a good percentage when the process is repeated five times. Additionally, the amount of dye adsorption decreased from 4.72 mg/g to 3.75 mg/g, which shows that 0.01 g of nanoparticles has the ability to be used repeatedly several times but that its effectiveness decreases in small amounts when the process is repeated repeatedly as shown in the Figure 3.9.



(3.8): The five-fold elimination of dye by Fe_3O_4 nanoparticles in the presence of cetramide

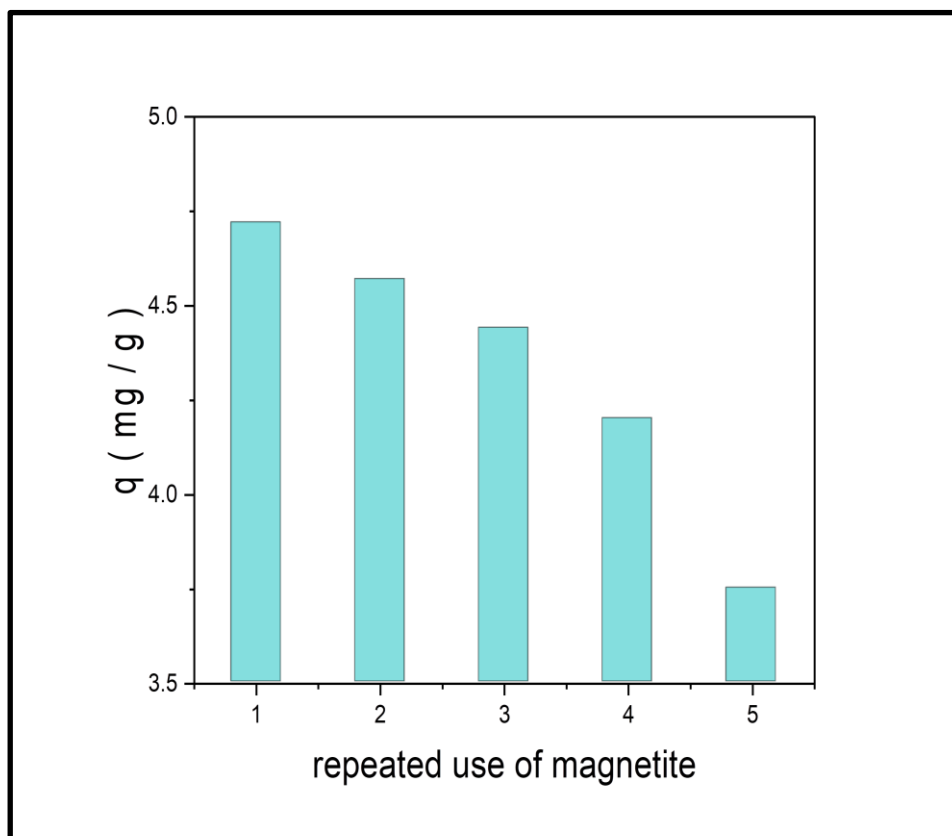


Figure (3.9): The correlation between the amount of substance that adsorbs on Fe_3O_4 nanoparticle sizes in presence of a cetramide in mg/g while utilizing Fe_3O_4 nanoparticle sizes in presence of a cetramide repeatedly.

3.6. Suggested mechanism of effect using surfactant on the adsorption

Based on the outcomes of produced experiments, Fig. 3.10 presents the proposed mechanism for the Fe_3O_4 nanoparticles coated with the produced cationic surfactant, cetramide in addition the dye. When using a cationic surfactant, the positive head group of the surfactant's molecules may electrostatically bind to the negative surface of the magnetite particles, causing the surfactant to be particularly adsorbed there. As a result of the surfactant's polar head (hydrophilic) and non-polar tail (hydrophobic) as in Fig. 3.10, it is shown that the surfactant molecules align themselves with the hydrophilic magnetite particles, adsorb on their surface also since the hydrophobic end is surrounded around Fe_3O_4 nanoparticles and the charged end is in water, the negatively charged particles of the dye are attracted to

the positive end of the cetramide, and leave a clear space between the head groups and the magnetite particles. The reverse micelles method is basically a water-in-oil emulsions that generate reverse micelles, which act as nonreactors for various physico-chemical processes. In this particular case, a reverse micelle solution is created by inversion of typical surfactant micelles, which encourages the creation of reverse micelles. On the other hand, it has been demonstrated that the ionic surfactant micelles' lifetime in aqueous solution, i.e. the characteristic micellization-dissolution equilibrium time noticeably increases with increasing hydrophobic tail length [86-88].

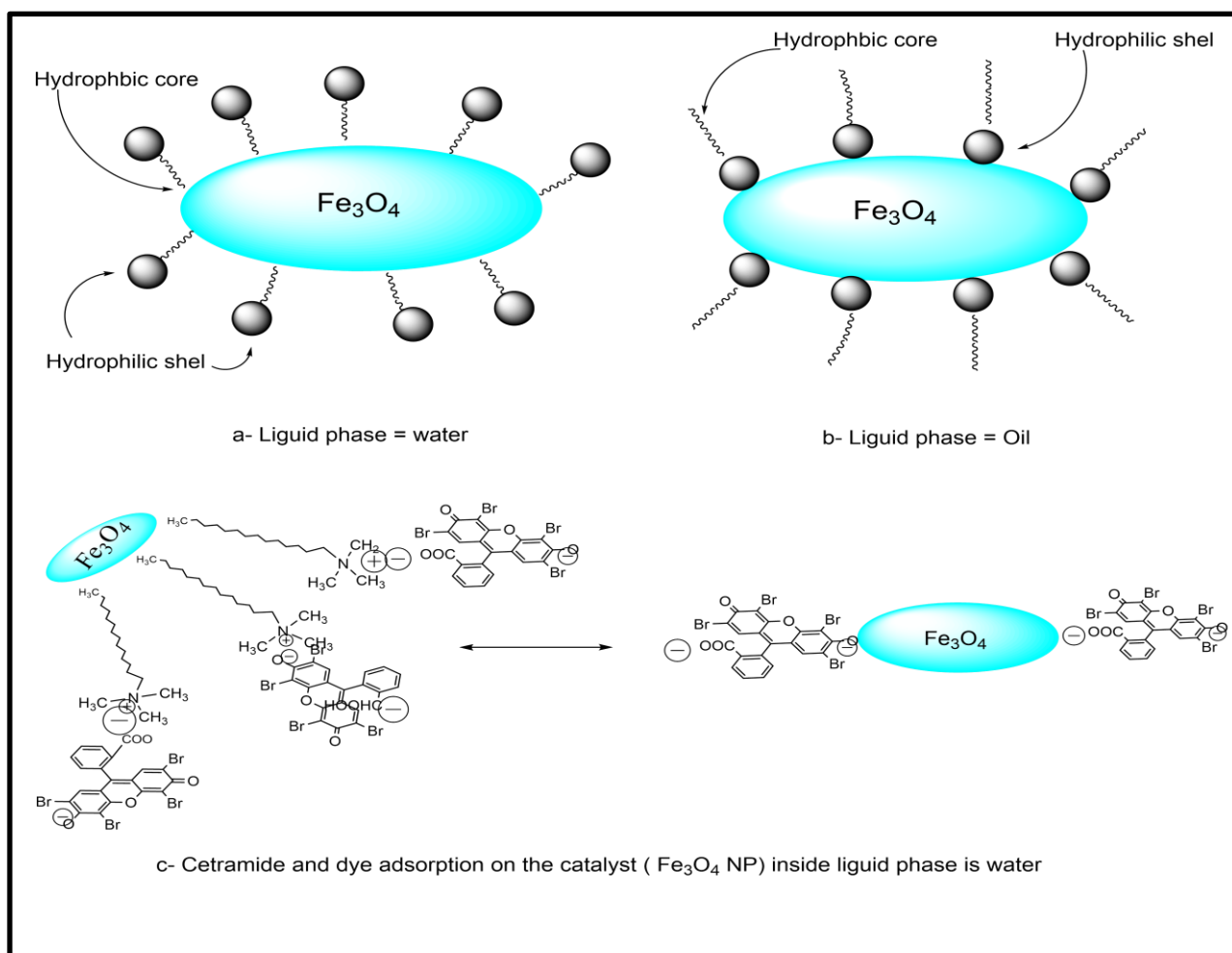


Figure (3.10): Referring to Adsorption of the surfactant and dye on the catalyst (Fe_3O_4 NP) and Micelle and Reverse Micelle Solutions Schematic, taken from this source.

3.7. Study Factors influencing on Removal of Eosin yellow Dye from aqueous solution

This part includes clarification of some factors that affect the use of Fe₃O₄ in removing Eosin yellow dye that pollute water. In addition, the work includes adsorption isotherms, theoretical models that describe isotherms and thermodynamic functions of the adsorption process and factors include:

3.7.1. Equilibrium Time of Adsorption System

In order to ascertain of time needed to achieve equilibrium between the adsorbent surface and the adsorbent because of the time is from the parameters that impact the E%, in which a concentration of 10 mg/L and a surface weight (Fe₃O₄) of 0.01 g for the dye were inserted. Shake for intervals of 10, 20, 30, 40, 50, and 60 minutes at laboratory temperature (298K). The absorbance was then determined at the dye's maximum wavelength, 516 nm, after the magnetite NP had been separated using a magnet. The results shown in Figure 3.11 and table 3.1, demonstrate that the time 60 min is the best equilibrium time for Eosin dye because it reaches an equilibrium state where all of the active sites in the adsorption material have been occupied by the dye separately by forming hydrogen bonds with the oxygen ions present on the surface of the adsorbent material. This was fixed in subsequent experiments.

Table 3.1. The removal percentages of Eosin yellow dye from aqueous solutions using Fe₃O₄ surface at different times and 298 K

Time/min.	Removal% = $(\frac{C_0 - C_e}{C_0} \times 100)$
10	78.177
20	80.359
30	84.595
40	86.777
50	91.270

60	94.480
----	--------

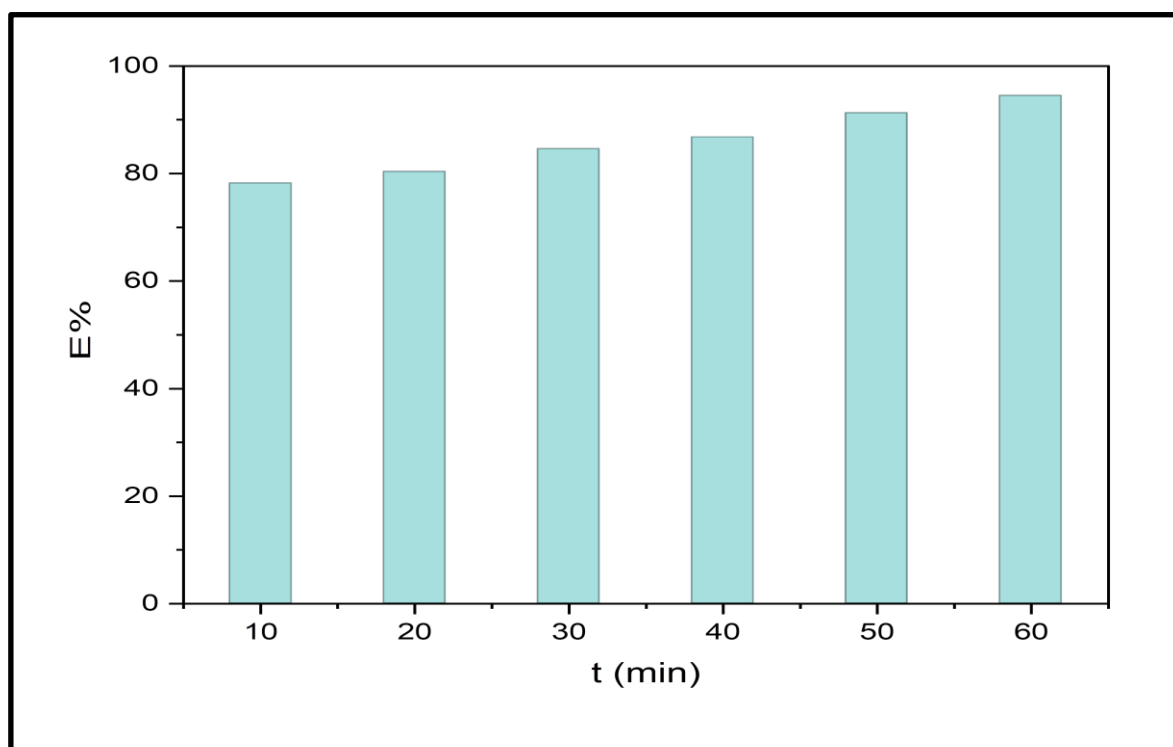


Figure (3.11): Effecting of equilibrium time on removal efficiency % of Eosin yellow dye

3.7.2. Effect of the Weight of Surface Adsorbent

The removal of the Eosin yellow dye is affected by changes in the weight of the adsorbent surface (magnetite NP), so this effect was investigated using concentration (10 mg/L), an equilibrium time (60 min.) of the amount, and at a temperature of 298 K with the use of various weights of the adsorbent surface that ranged between (0.005, 0.01, 0.02 and 0.03) g at 298 K and pH 6.5, as is Fig.3.12. Table 3.2. Due to the availability of a larger surface area with an increase in the number of active sites prepared for adsorption, the percentage of dye removal ($E_{\%}$) rises with the weight of the adsorbing surface [89], which in turn causes an increase in the amount of Eosin yellow dye being adsorbed from the solution.

The amount of adsorbent material in the saturation stage, which means that the surface is saturated with the adsorbent and is not affected by an increase in the weight of the adsorbent surface (Fe_3O_4), is represented by the removal percentage ($E\%$), which increases until it reaches a specific value, and it constant means that the amount is constant. Therefore, the weight of 0.01 g provided the best adsorption rate for the dye. Discovered that 0.01 g was the best due to the $E\%$ in the other weights was slightly raised in comparison to 0.01 g, and we also took into account the cost of the manufactured Fe_3O_4 NP.

Table (3.2): Explaining Eosin dye removal percentages from aqueous solutions employing various weights from the surface of Fe_3O_4 NP at 298 K

Wt. (g)	Removal% = $\left(\frac{C_o - C_e}{C_o} \times 100\right)$
0.005	80.231
0.01	94.500
0.02	95.000
0.03	96.000

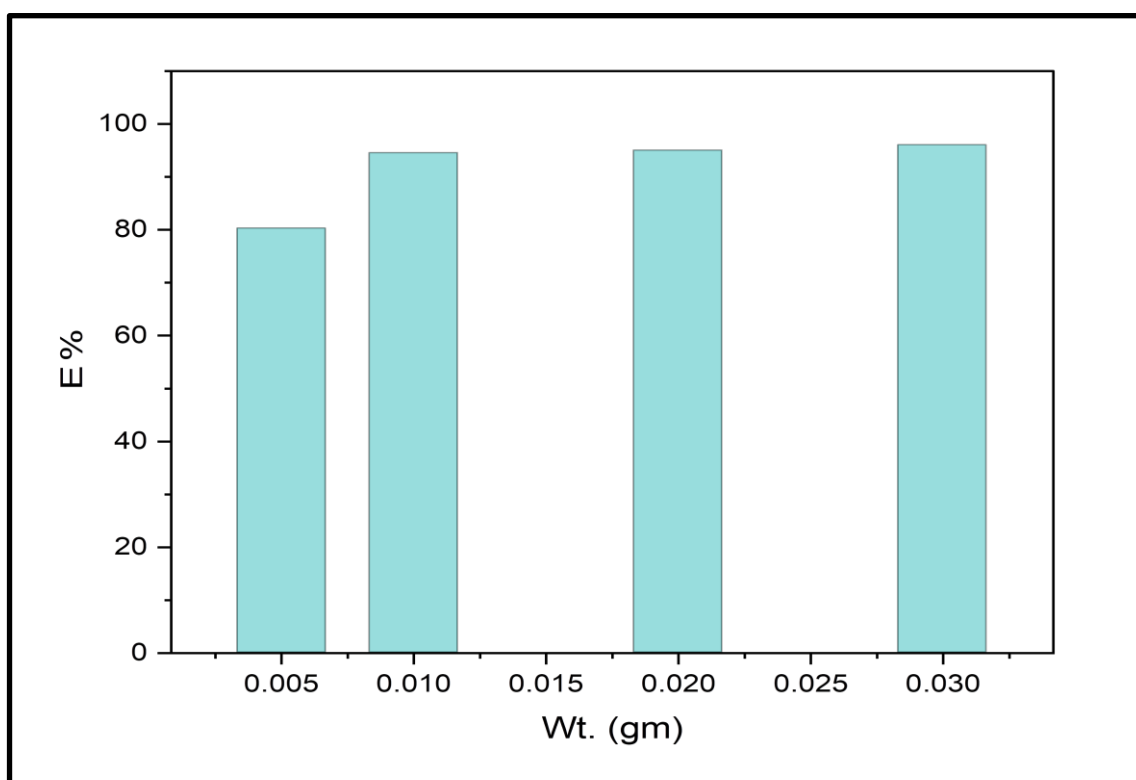


Figure (3.12): Effecting of surface weight of Fe₃O₄ on clearance rate of Eosin yellow dye

3.7.3. Effect of pH

One of the key factors influencing the dye and process of the removal the dye from its solutions is pH, often which that effect on the resonance of the dye (mesmeric effect) of the dyes which caused to shifting the colors from medium to other therefore was studied the effecting the pH and applied the removal percent (% E). With pH, adsorbate's chemical properties change. The degree of ionization and speciation of different dyes is influenced by the pH of the solution, which ultimately changes the reaction kinetics and equilibrium properties of the adsorption process. Fig.3.13 and table (3.3) displays the E removal % of dye removal at various pH values for an initial dye concentration of 10 mg/L. % E is significantly impacted by pH. modifying the chemistry of the dye molecules as well as the surface of Fe₃O₄ NP inside aqueous solutions. As a dipolar of Eosin yellow dye when it in the low pH molecules. Eosin yellow dye contains a carboxylic group, carbonyl groups and phenolic groups. These groups are naturally nucleophilic [90]. The dye is released when the pH of the dye solution drops. Protonated molecules are removed on the surface of the magnetite produced by the surfactant cetramide. This figure shows that for an initial dye concentration of 10 mg/L, removal % was approximately 60.20 % at pH 3, 61.85% at pH 5, and a higher value of % E_{elimination} was 95.68% at pH 6.5. (pH of the dye), pH elevation resulted in a decrease in % E_{removing}. Using a 10 mg/L starting dye concentration, the removal percentage was 38.87 % at pH 9 on other hand it a negligibly low 14.65 % at pH 12, because the active sites were occupied by OH⁻ groups and there was a repulsion between the OH⁻ groups of the dye and iron nanoparticle as the Fig 3.14, the basic medium had no effect on the dye concentration and the removal % was very low.

Table (3.3): Eosin dye removal percentages from aqueous solutions using the surface of Fe₃O₄ NP at various initial pH and at 298 K

pH	Removal% = $(\frac{C_o - C_e}{C_o} \times 100)$
3	60.201
5	61.853
6.5	95.681
9	38.874
12	14.657

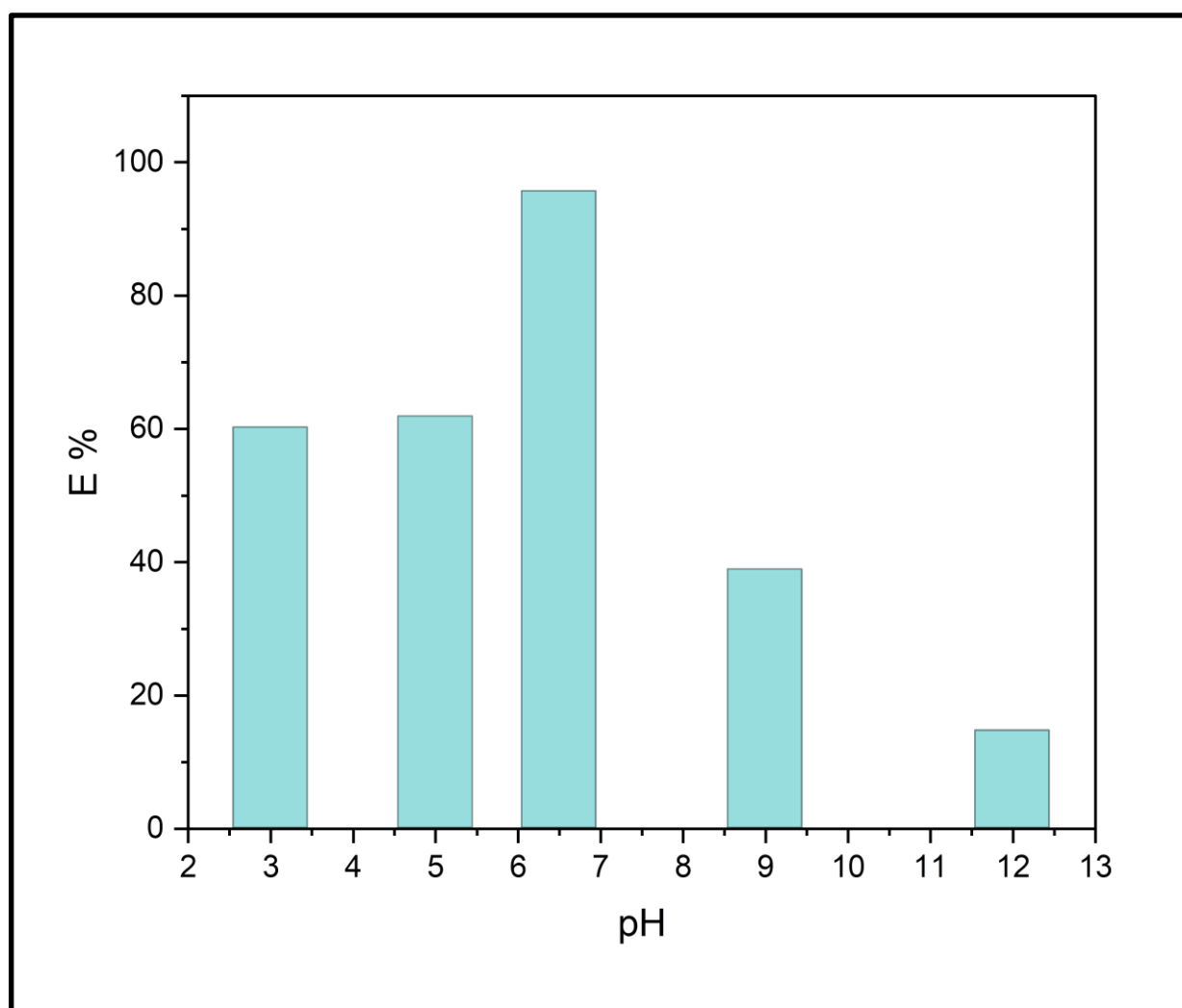


Figure (3.13): Effecting of pH on the desorption of Eosin yellow dye.

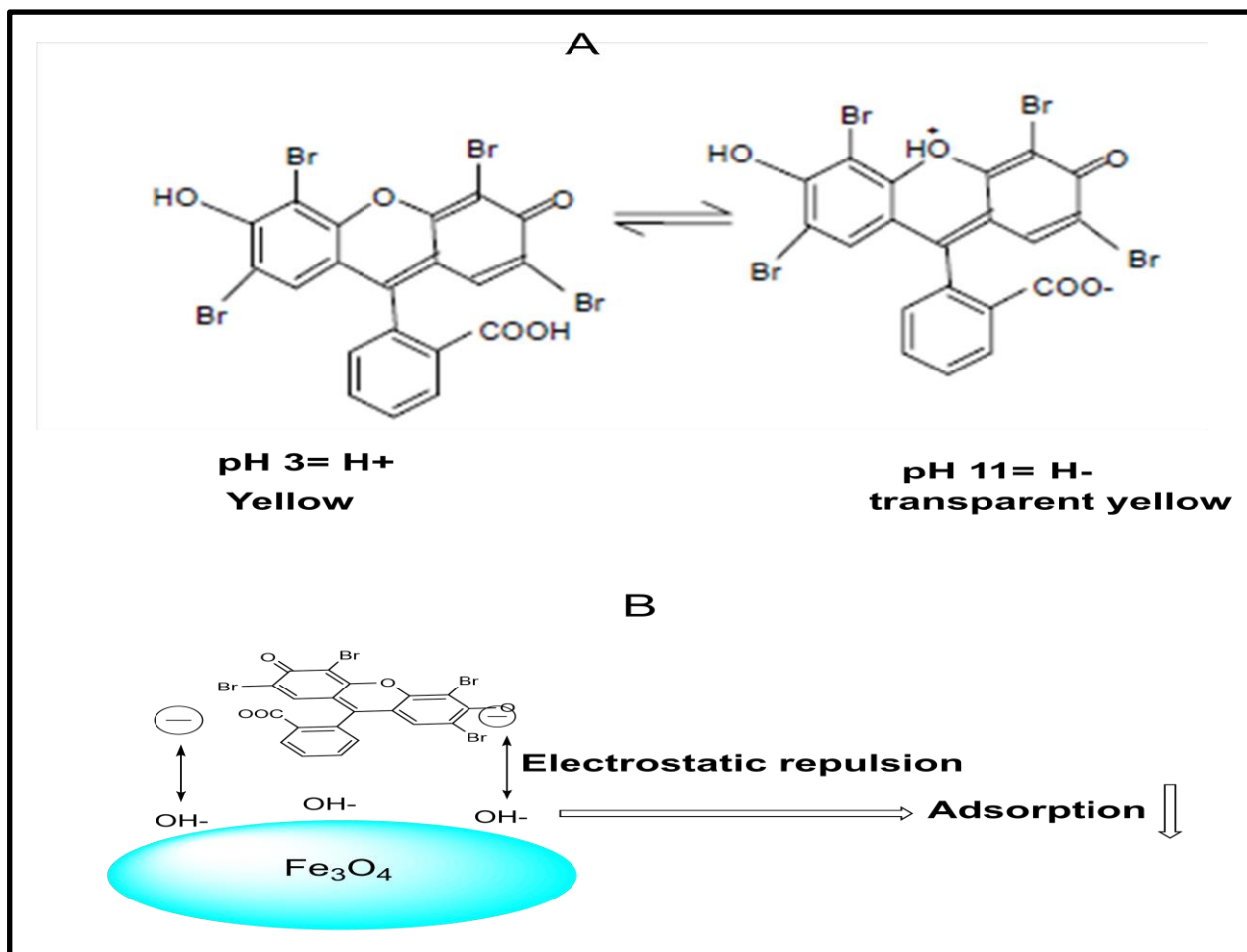


Figure (3.14): (a) Structure of eosin in acidic and basic medium adapted from this references [91, 92] and (b) Schematic for repulsion of OH groups onto iron oxide NP modified from this reference [93]

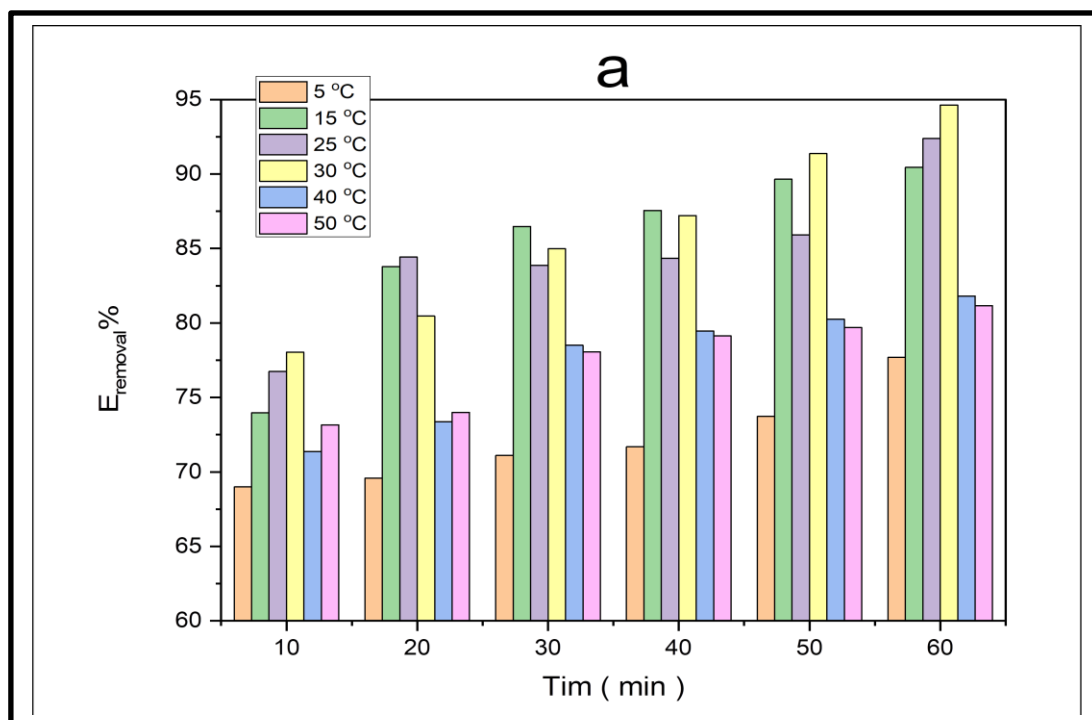
3.7.4. Effect of Temperature on Removal of Dye

Temperature can have an impact on both the structure of the dye and how well it is removed by magnetite nanoparticles. Therefore, the influence of temperature from (278 to 323) K on the incubation duration of (10 to 60) minutes, the dye employed, the % $E_{\text{elimination}}$ and q_e were evaluated. According to the data in figure 3.15, table (3.4), the removal values rise as the temperature rises. This behavior shows that as the temperature rises, dyes become more mobile and have higher kinetic energies, making it easier for them to reach the surfaces of active sites. It

also shows that as pores become larger and depigment, the dyes' propensity for adsorption on catalyst surfaces increases [84, 94]. Higher value of $E_{\%}$ and q_e was in 303 K. On the other hand, at high temperatures like 313 K and 323 K, the $E_{\text{removal}\%}$ falls. This is the reasoning behind the dye concentration with vaporization of the aqueous solutions.

Table (3.4): Referring to Eosin dye removal percentages from aqueous solutions by using various weights from the surface of Fe_3O_4 NP at 298 K

Time/min.	Removal% = $(\frac{C_0 - C_e}{C_0} \times 100)$
5	77.692
15	90.439
25	92.375
30	94.625
40	81.170
50	81.100



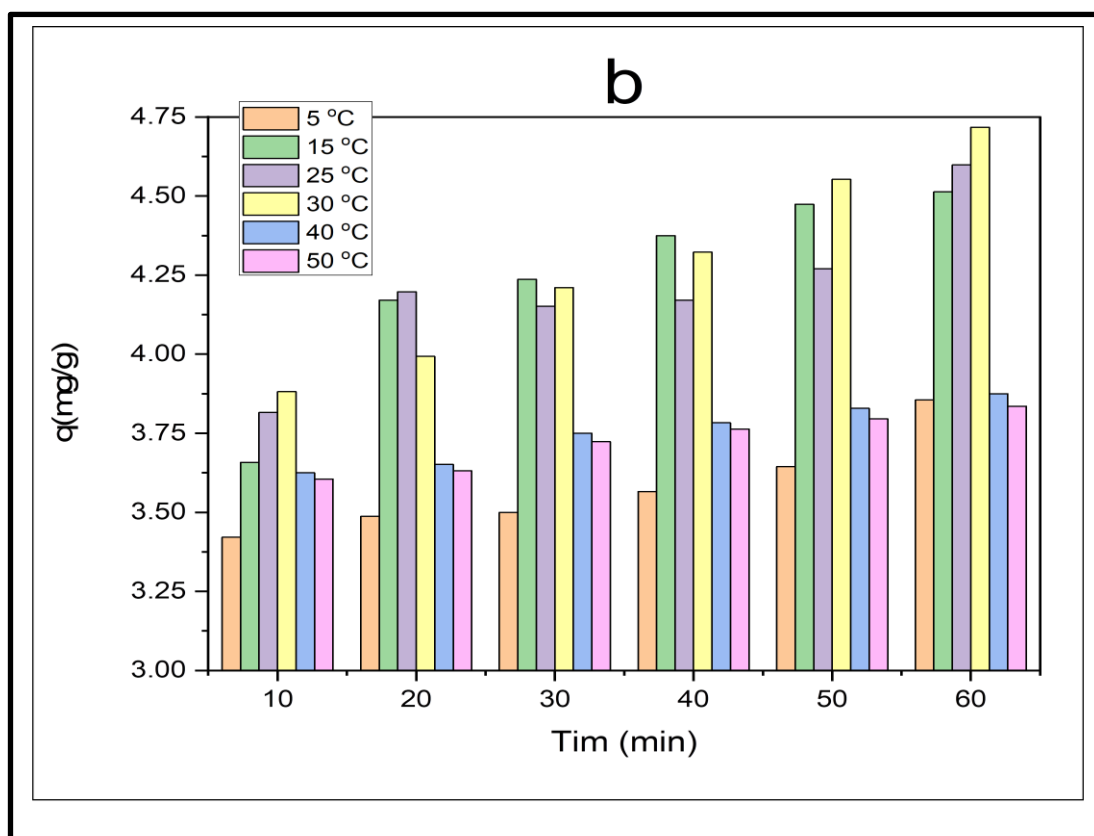


Figure (3.15): The impact of temperature on the efficacy of iron oxide nanoparticles (NP) produced in the presence of cetramide surfactant in the removal of dye (a) $E\%$ with the time (b) q_e with the time.

3.8. Thermodynamics parameters

In order to investigate the type of adsorption process that occurred on any solid surface, thermodynamics parameters are essential. Equation (1.11) was used to initially determine the sorption distribution coefficient (k_d) [94, 95], C_{ads} is the amount of adsorbate (dye) on the solid surface (Fe_3O_4 in presence and absence cetramide) and C_e is a residual dye (mg/L) in a solution at equilibrium. Used the equations (1-10 to 1-14) to determining thermodynamics factors. Comparison kinetic and Thermodynamic between magnetite NP produced by cetramide and Fe_3O_4 without cetramide as shown in table 3.5 is based on the results in figures 3.16 and 3.17 as well as table 3.6., for adsorption isotherms magnetite with and without surfactants.

Table (3.5): The Thermodynamic Parameters for eosin yellow dye adsorption on Fe_3O_4 surface prepared in presence and absence cetramide at (278-303) K.

Adsorbate	(1000/T)	Ln k_d	ΔH° kJ mol ⁻¹	ΔS° kJ mol ⁻¹	ΔG° kJ mol ⁻¹	T/K	E_a kJ mol ⁻¹
Fe ₃ O ₄ in presence cetramide	3.597	-1.053	36.729	0.144	-3.273	278	39.040
	3.472	-2.091			-5.463	288	39.124
	3.355	-2.305			-6.134	298	39.207
	3.300	-2.684			-7.122	303	39.248
Fe ₃ O ₄ in absence cetramide	3.472	1.022	-149.827	-0.507	27.119	278	-147.433
	3.412	0.158			27.673	293	-147.391
	3.355	-1.177			28.229	298	-147.349
	3.300	-1.970			28.787	303	-147.308

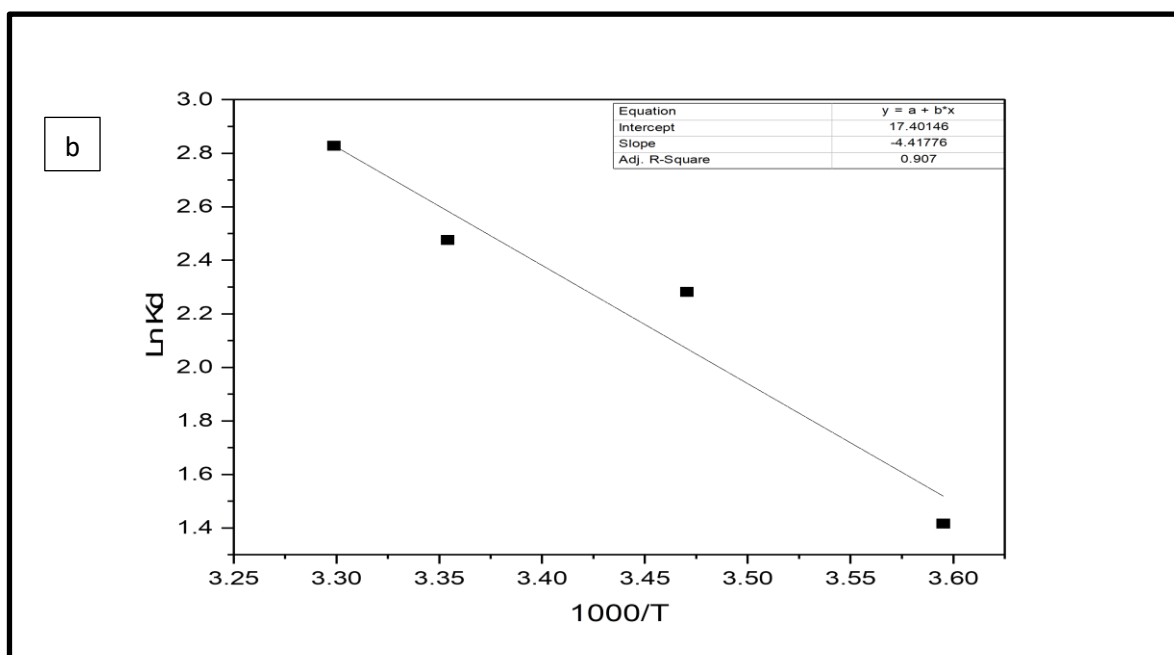
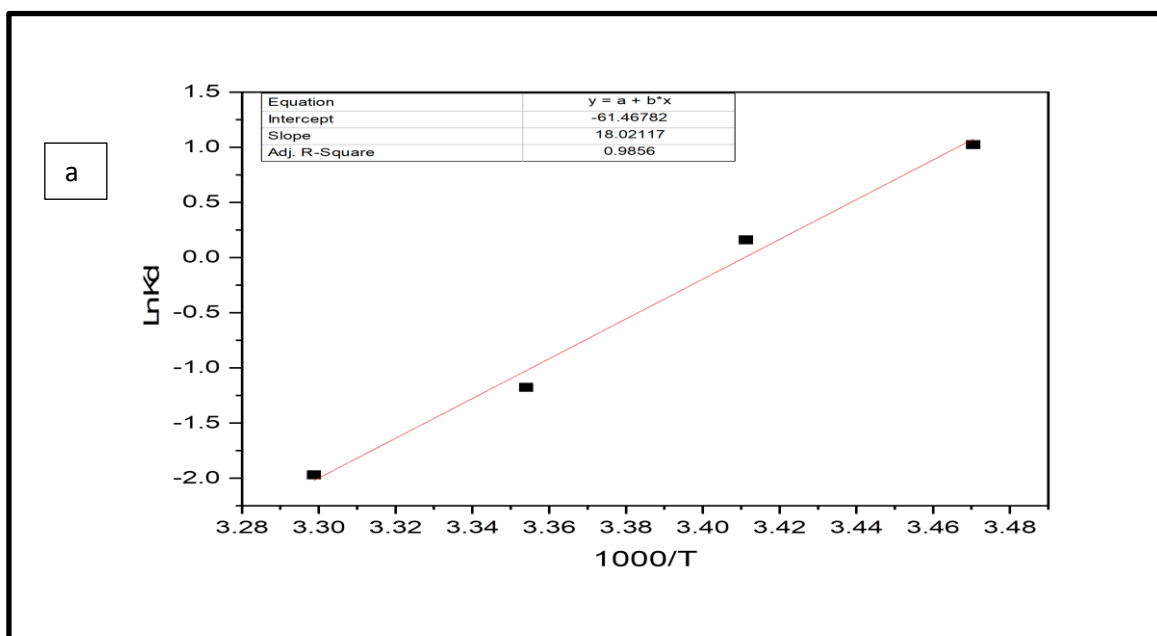


Figure (3.16): Compares the form relationship between Eosin yellow dye that was adsorbed on Fe_3O_4 surface (a) in the absence of cetramide and (b) in the presence of cetramide as a surfactant at 1h.

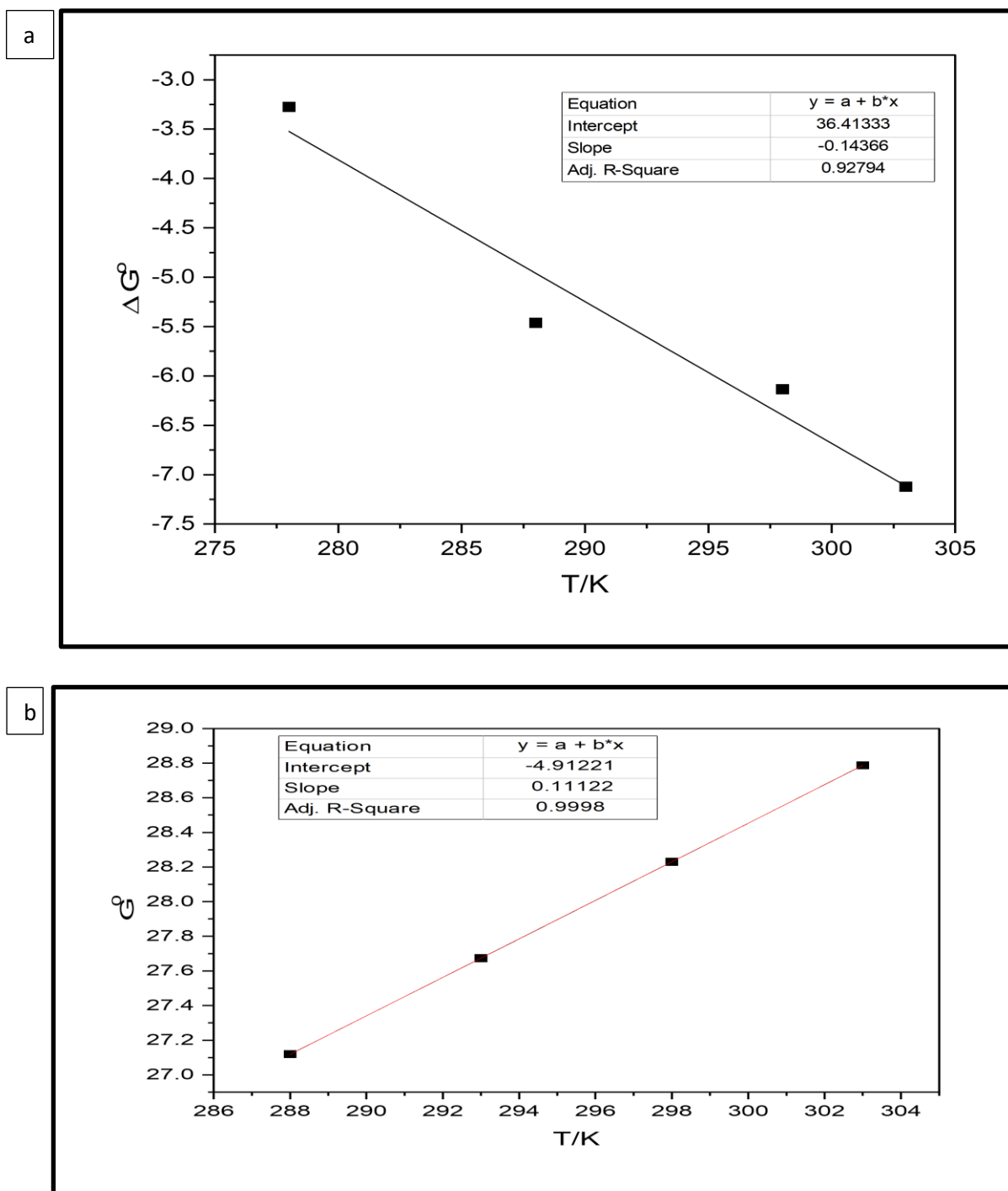


Figure (3.17): Referring to Gibb's free energy change (ΔG^0) versus temperature for (a) Fe_3O_4 with cetramide (b) magnetite without cetramide

Table (3.6): Comparing the adsorption isotherms for Fe₃O₄ surfaces produced with and without cetramide

Fe ₃ O ₄ with cetramide	Fe ₃ O ₄ without cetramide
It has a positive ΔH° (36.729 kJ mol ⁻¹) magnitude and is endothermic in nature.	It is exothermic and has a negative ΔH° (-149.827 kJ mol ⁻¹) magnitude.
Chemisorption is a method because ΔH° is more valuable than (20) kJ mol ⁻¹ [34]	Physisorption is a method because ΔH° is lower than (20) kJ mol ⁻¹
ΔS° magnitudes is modest and positive (0.14467 kJ mol ⁻¹) that implies the solid/solution interface becomes more random; as a result, the adsorption mechanism occurs as an associative mechanism with changes in the internal structure [34, 96].	Inferring that the ΔS° for solid/solution interface becomes lower randomness therefore the value is lowest and negative (-0.5073 kJ mol ⁻¹).
the positive activation energy values rise as the temperature rises from (39.040 to 39.248) kJ mol ⁻¹	As the temperature increases, the negative activation energy values increase from (-147.433 to -147.308) kJ mol ⁻¹ .
As a result of the activation energies value being between (8.4 and 83.7) kJ mol ⁻¹ therefore it is chemisorption process [34].	Because the activation energies are not between 8.4 and 83.7 kJ mol ⁻¹ , the process is physisorption.
The fact that the negative ΔG° magnitudes decreased as the temperature rose suggests that the reaction is favorably spontaneous and does not require energy from an external source to transform reactants into products. The magnitudes ranged from (-7.122 to -3.273) kJ mol ⁻¹ [34], so previously reported findings of a similar nature concur with the thermodynamics findings[94].	Given that the positive ΔG° magnitudes grew as the temperature increased, it seems unlikely that the reaction is favorable and spontaneous.

3.9. Isotherm Models in Difference of Concentration in ppm

In this study, we tried to using the isotherm equations given by Freundlich, Langmuir and Temkin in presence of the difference concentrations, to fit the revealed experimental data for Eosin dye removing. The relationship between the amount of dye that has been removed and the dye concentration that is still present at equilibrium is expressed by the adsorption isotherm [97]. In this study, the non-linear Langmuir and Freundlich models were fitted to experimental data from adsorption isotherms to describe the adsorption process. The monolayer adsorption of the adsorbate on certain homogenous sites inside the adsorbent is described by:

3.9.1. Langmuir model as the figure 3.18 provides the nonlinear Langmuir model's expression. Utilizing Langmuir isotherms to compare magnetite with and without cetramide allowed for the analysis of the experimental adsorption data. Using the correlation coefficient R^2 , the applicability of various isotherms was compared. Table 3.7 contains the values for the other isotherm parameter. The examined adsorption isotherms in the instance of Fe_3O_4 NP that was produced with cetramide corresponded to experimental data, as seen in Table and based on the R^2 values [98].

Table (3.7): Compares the Fe_3O_4 without and with cetramide in the Langmuir models

Models	Langmuir for Fe_3O_4	Langmuir for Fe_3O_4 + cetramide
K_L (L/mg)	1.60×10^2	-120.403
q_{max} (mg/g)	244.498	0.431
R^2	0.4952	0.6406

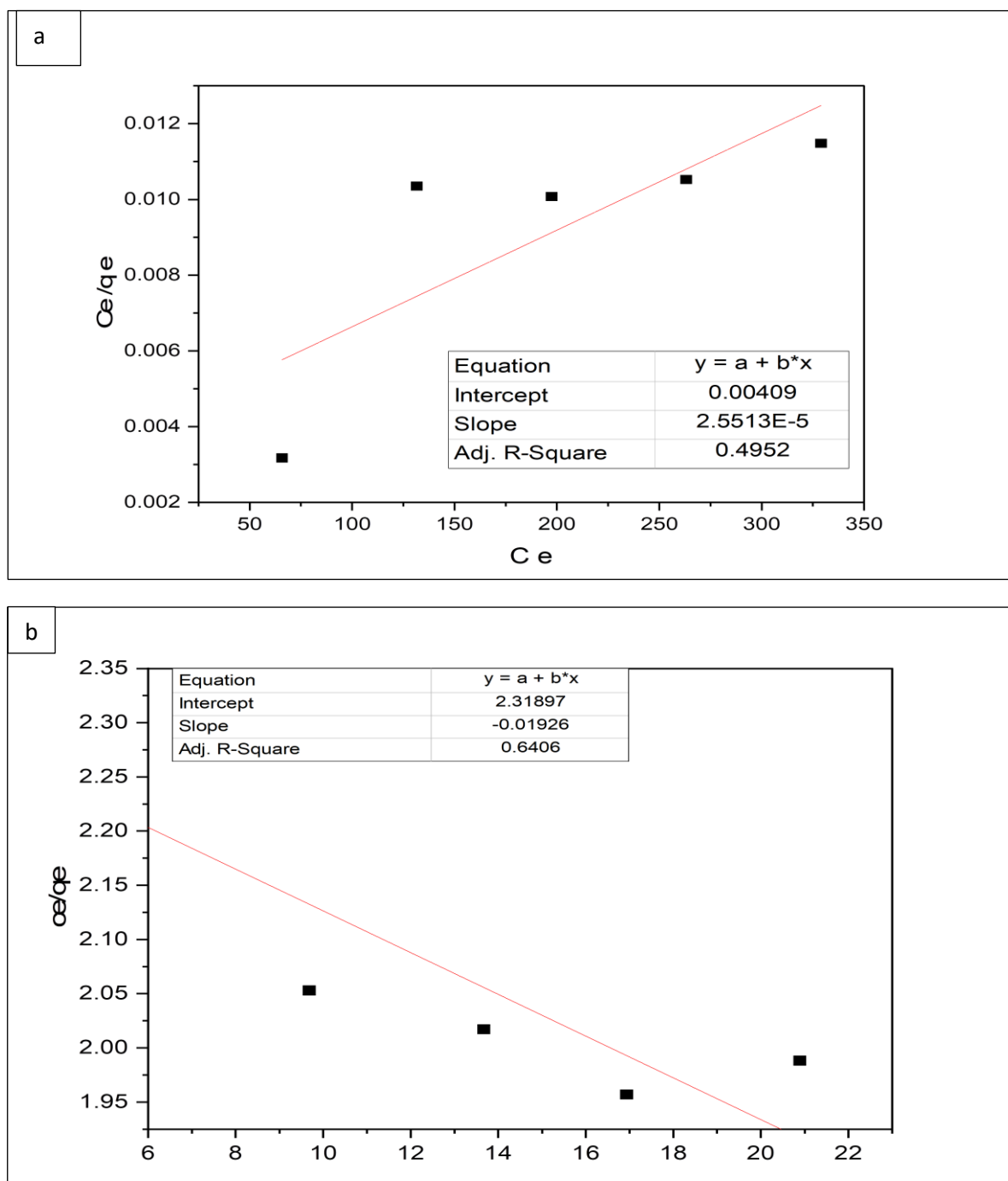


Figure (3.18): Plots of the Langmuir equation for Fe_3O_4 NPS in (a) and Fe_3O_4 NPS in (b) the presence of cetramide.

3.9.2. Freundlich isotherms

The experimental adsorption results were analyzed by comparing magnetite with and without cetramide using the Freundlich. Using n and the R^2 correlation

coefficient, It is more closely followed than the Langmuir equation when dye is adsorbed on produced Fe_3O_4 using cetramide, as evidenced by the n value being close to 1. This suggests chemisorption. As depicted in figure 3.19 and detailed in table 3.8, It is discovered that the processes of physical adsorption for Fe_3O_4 without cetramide and chemical adsorption for employing produced Fe_3O_4 with cetramide as surfactant.

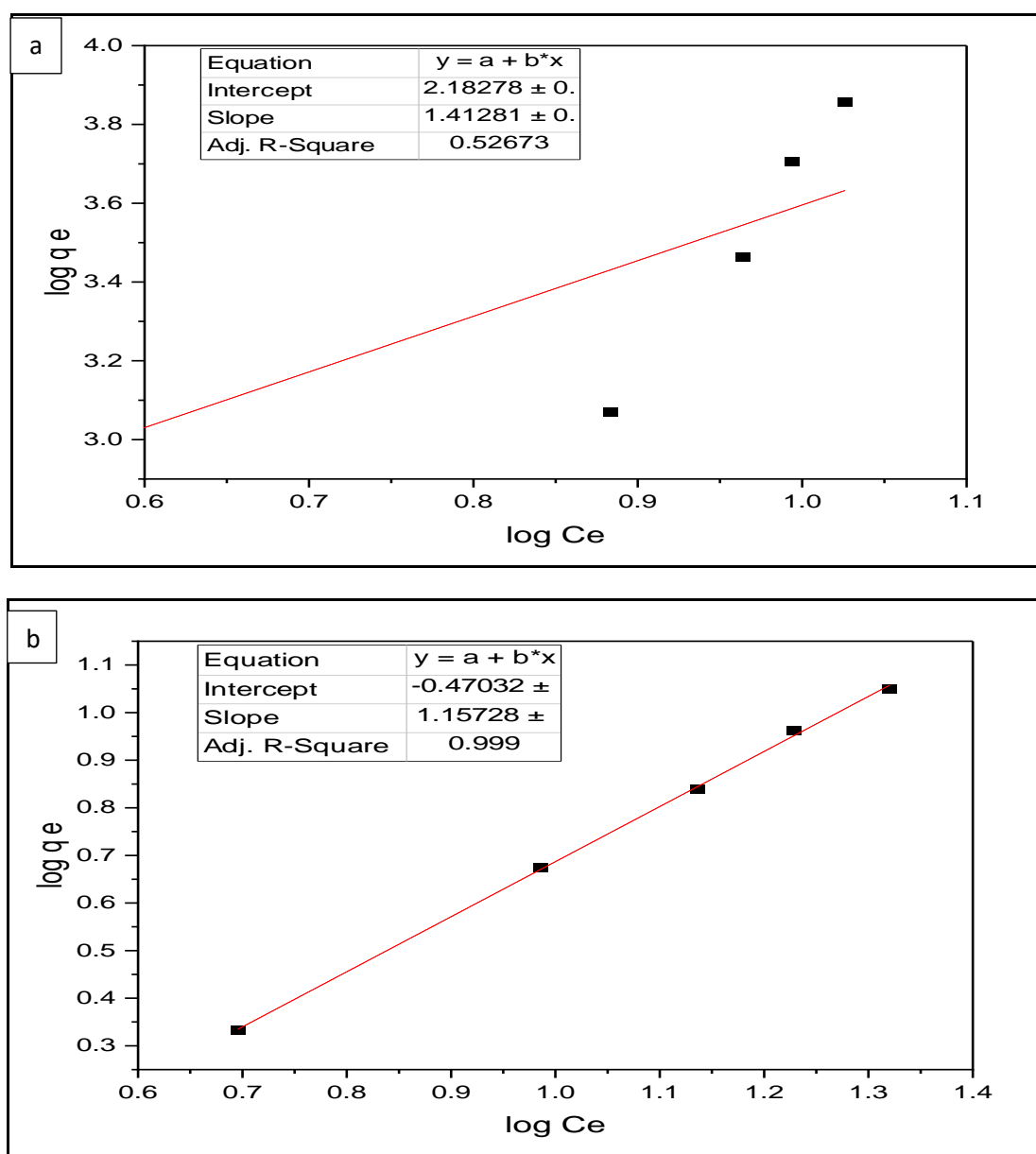


Figure (3.19): Plots of the Freundlich equation for Fe_3O_4 NPS in (a) and Fe_3O_4 NPS with cetramide in (b).

Table (3.8): Comparative Freundlich models for Fe₃O₄ without and with cetramide as the surfactant

Models	Freundlich equation for Fe ₃ O ₄	Freundlich equation for Fe ₃ O ₄ + cetramide
$K_f=(\text{mg g}^{-1})(\text{L mg}^{-1})^{1/n}$	152.328	0.338
n (g/L)	1.283	0.864
R ²	0.526	0.999

3.9.3. Temkin isotherm: It used in the analysis of the experimental adsorption data to compare magnetite with and without cetramide in figure 3.20. The correlation coefficient R² was used to compare these isotherms' applicability. The values for the isotherm constants A and B are compiled in Table. It is evident from Table 3.9 and based on the R² values that the considered adsorption isotherms in the case of Fe₃O₄ that was produced with cetramide matched experimental data.

Table (3.9): Constant values of Temkin equation

Models	Temkin Equation for Fe ₃ O ₄	Temkin Equation for Fe ₃ O ₄ + cetramide
B	0.704	6.175
KT	0.041	0.255
R ²	0.5013	0.9304

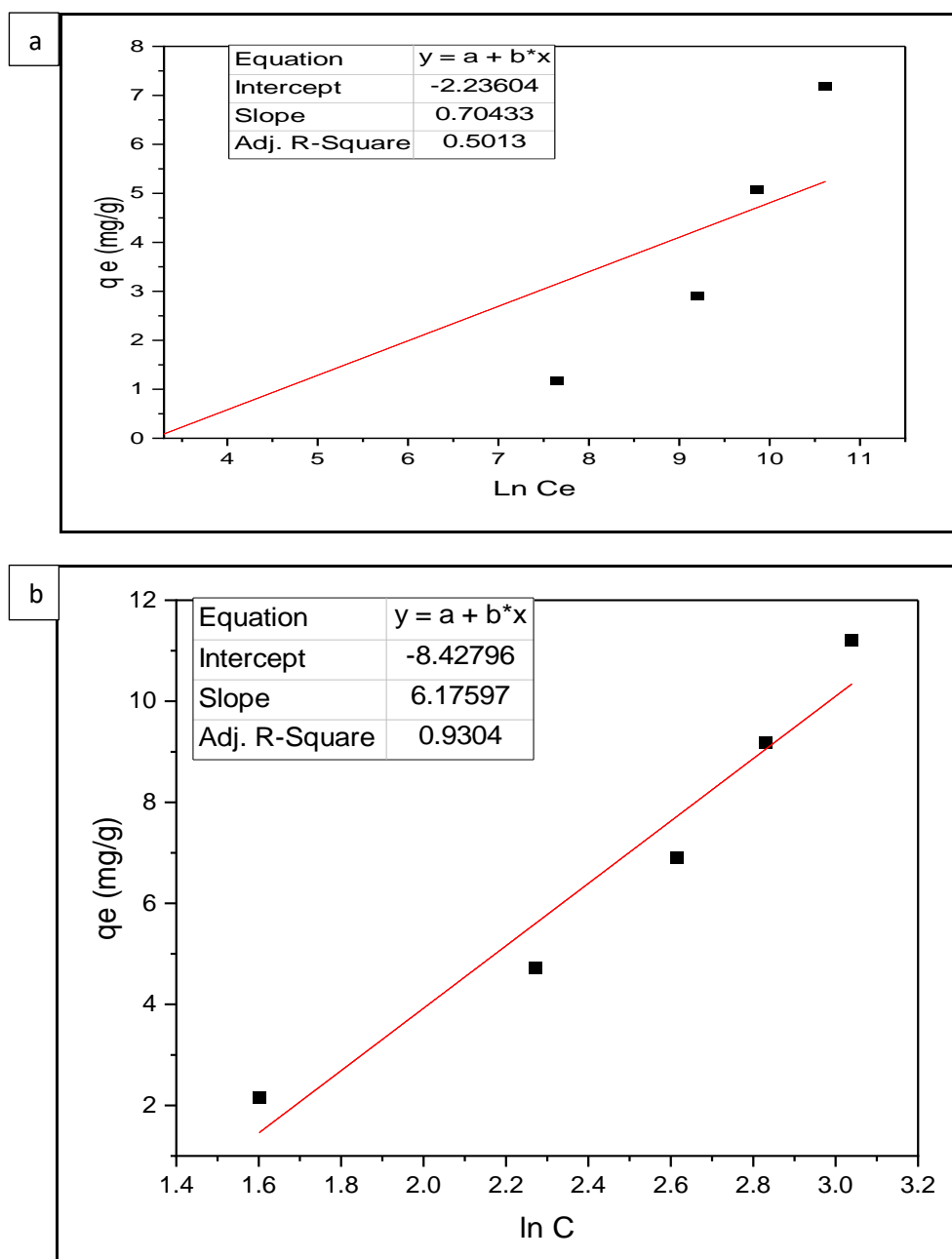


Figure (3.20): Plots of the Temkin equation for Fe_3O_4 NPS in (a) and Fe_3O_4 NPS with cetramide in (b).

3.10. Conclusions

Based on the empirical study was conducted, the following conclusions were reached:

1. It was found that the preparation of iron oxide nanoparticles with surfactants had a higher efficiency than iron oxide nanoparticles that prepared without a surfactant.
2. Characterization techniques such as XRD, FT-IR and SEM showed the success of preparing iron oxide nanoparticles without and with using surfactants.
3. All prepared samples found as nanomaterials with irregular spherical shapes that aggregated together like- broccoli.
4. The FT-IR analysis demonstrated the Fe-O octahedral and tetrahedral bending Peaks, and all samples are inverse spinel.
5. The mean crystal size of iron oxide nanoparticles arises after addition of various surfactants as template.
6. The using of Fe_3O_4 NPs as magnetic adsorbents was successes and economy for removing the eosin yellow dye from aqueous solutions.
7. The best adsorbent material for removing eosin yellow dye is (Fe_3O_4 + cetramide) that given higher removal percentage compared to other iron oxides nanoparticles for 60 minutes.
8. The neutral medium (pH 6.5) is given a best removal of eosin yellow.
9. The removal efficiency increases with the increase in temperature as a result of the increase in kinetic energy.
10. The thermodynamic study showed that the process of adsorption of iron oxide nanoparticles with cetrimide is an endothermic process, spontaneous and

chemisorption, but without cetramide the adsorption is physical with exothermic process and spontaneous .

11. Isotherm study explains that ($\text{Fe}_3\text{O}_4 + \text{CT}$) is applying on Langmuir, Freundlich and Temkin models contrary magnetite without cetramide .

3.11. Future Studies

1. Preparation of iron oxide nanoparticles using environmentally friendly methods, being less expensive and non-toxic, and bonding the nanoparticles with other surfactants.
2. Characterization of the prepared surfaces using other techniques such as atomic force microscope (AFM), thermo gravimetric analysis (TGA), BET surface area, and Raman spectroscopy, to identify the surface area, the active sites on the surface and the thickness of the nano-layer.
3. Studying the effect of other factors on the adsorption process, such as ionic strength, surfactants concentration, and shaking speed.
4. Study the biological activity of prepared materials.
5. Study the mechanical and electrical properties of prepared materials.

References

References

References

1. Appannagari, R.R., *Environmental pollution causes and consequences: a study*. North Asian International Research Journal of Social Science and Humanities, 2017. **3**(8): p. 151-161.
2. Khan, M.A. and A.M. Ghouri, *Environmental pollution: its effects on life and its remedies*. Researcher World: Journal of Arts, Science & Commerce, 2011. **2**(2): p. 276-285.
3. Vesilind, P.A., J.J. Peirce, and R.F. Weiner, *Environmental pollution and control*. 2013: Elsevier.
4. Owa, F., *Water pollution: sources, effects, control and management*. International Letters of Natural Sciences, 2014. **3**.
5. Gita, S., A. Hussan, and T. Choudhury, *Impact of textile dyes waste on aquatic environments and its treatment*. Environ. Ecol, 2017. **35**(3C): p. 2349-2353.
6. Ali, H., *Biodegradation of synthetic dyes—a review*. Water, Air, & Soil Pollution, 2010. **213**(1): p. 251-273.
7. Hassaan, M.A., A. El Nemr, and A. Hassaan, *Health and environmental impacts of dyes: mini review*. American Journal of Environmental Science and Engineering, 2017. **1**(3): p. 64-67.
8. Padhi, B., *Pollution due to synthetic dyes toxicity & carcinogenicity studies and remediation*. International journal of environmental sciences, 2012. **3**(3): p. 940-955.
9. Zhou, Y., J. Lu., Y. Zhou., Y. Liu., *Recent advances for dyes removal using novel adsorbents: a review*. Environmental pollution, 2019. **252**: p. 352-365.
10. Sarkar, S., A. Banerjee., U. Halder., R. Biswas., *Degradation of synthetic azo dyes of textile industry: a sustainable approach using microbial enzymes*. Water Conservation Science and Engineering, 2017. **2**(4): p. 121-131.
11. Kasbaji, M., M. Mennani., N. Grimi., F.J. Barba., *Implementation and physico-chemical characterization of new alkali-modified bio-sorbents for cadmium removal from industrial discharges: Adsorption isotherms and kinetic approaches*. Process Biochemistry, 2022. **120**: p. 213-226.
12. Turku, I., *Adsorptive removal of harmful organic compound from aqueous solutions*. 2010: Lappeenranta University of Technology.
13. Schoutteten, K., *Adsorption of Pharmaceuticals on Activated Carbon, Measurements, Mechanisms, and Modelling*. 2012, Master's thesis, Universiteit Gent.
14. Atkins, P. and J. De Paula, *Elements of physical chemistry*. 2013: Oxford University Press, USA.
15. Bruch, L.W., M.W. Cole, and E. Zaremba, *Physical adsorption: forces and phenomena*. 2007: Courier Dover Publications.
16. Bello, A., K. Makgopa., M. Fabiane., D. Dodoo.Ahrin., *Chemical adsorption of NiO nanostructures on nickel foam-graphene for supercapacitor applications*. Journal of materials science, 2013. **48**(19): p. 6707-6712.
17. Tighadouini, S., S. Radi, and Y. Garcia, *Selective chemical adsorption of Cd (II) on silica covalently decorated with a β -ketoenol-thiophene-furan receptor*. Molecular Systems Design & Engineering, 2020. **5**(6): p. 1037-1047.
18. Wibowo, N., L. Setyadi., D. Wibowo., J. Setiawan., *Adsorption of benzene and toluene from aqueous solutions onto activated carbon and its acid and heat treated forms: influence of surface chemistry on adsorption*. Journal of hazardous materials, 2007. **146**(1-2): p. 237-242.

References

19. Yagub, M.T., T.K. Sen., S. Afroze., H.M. Ang ., *Dye and its removal from aqueous solution by adsorption: a review*. Advances in colloid and interface science, 2014. **209**: p. 172-184.
20. Azizian, S. and S. Eris, *Adsorption isotherms and kinetics*, in *Interface Science and Technology*. 2021, Elsevier. p. 445-509.
21. Guo, X. and J. Wang, *A general kinetic model for adsorption: theoretical analysis and modeling*. Journal of Molecular Liquids, 2019. **288**: p. 111100.
22. Wang, J. and X. Guo, *Adsorption isotherm models: Classification, physical meaning, application and solving method*. Chemosphere, 2020. **258**: p. 127279.
23. Bozorgian, A., *Investigation and comparison of experimental data of ethylene dichloride adsorption by Bagasse with adsorption isotherm models*. Chemical Review and Letters, 2020. **3**(2): p. 79-85.
24. Ho, Y., J. Porter, and G. McKay, *Equilibrium isotherm studies for the sorption of divalent metal ions onto peat: copper, nickel and lead single component systems*. Water, air, and soil pollution, 2002. **141**(1): p. 1-33.
25. Ezzati, R., *Derivation of pseudo-first-order, pseudo-second-order and modified pseudo-first-order rate equations from Langmuir and Freundlich isotherms for adsorption*. Chemical Engineering Journal, 2020. **392**: p. 123705.
26. Said, K.A.M., N.Z .Ismail., R.L. Jama'in., N.A.M. Alipah., *Application of Freundlich and Temkin isotherm to study the removal of Pb (II) via adsorption on activated carbon equipped polysulfone membrane*. Int. J. Eng. Technol, 2018. **7**(3.18): p. 91-93.
27. Erdogan, F.O., *Freundlich, Langmuir, Temkin, DR and Harkins-Jura isotherm studies on the adsorption of CO₂ on various porous adsorbents*. International Journal of Chemical Reactor Engineering, 2019. **17**(5).
28. Nguyen, D.T., H.N. Tran., R.S. Juang., N.D. Dat., *Adsorption process and mechanism of acetaminophen onto commercial activated carbon*. Journal of Environmental Chemical Engineering, 2020. **8**(6): p. 104408.
29. Edet, U.A. and A.O. Ifelebuegu, *Kinetics, isotherms, and thermodynamic modeling of the adsorption of phosphates from model wastewater using recycled brick waste*. Processes, 2020. **8**(6): p. 665.
30. Hussain, S., M .Kamran., S.A. Khan., K. Shaheen., *Adsorption, kinetics and thermodynamics studies of methyl orange dye sequestration through chitosan composites films*. International journal of biological macromolecules, 2021. **168**: p. 383-394.
31. Alattar, R.A., H.M. Saleh., J.A .Al-Hilifi., *Influence the addition of Fe²⁺ and H₂O₂ on removal and decolorization of textile dye (dispersive yellow 42 dye)*. Egyptian Journal of Chemistry, 2020. **63**(9): p. 3453-3463.
32. Jaafar, M.T. and L.M. Ahmed. *Reduced the toxicity of acid black (nigrosine) dye by removal and photocatalytic activity of TiO₂ and studying the effect of pH, temperatue, and the oxidant agents*. in *AIP Conference Proceedings*. 2020. AIP Publishing LLC.
33. Saeed, S.I., B.H. Taresh., L.M. Ahmed., *Insight into the Oxidant Agents Effect of Removal and Photo-decolorization of Vitamin B12 Solution in Drug Tablets using ZrO₂*. Journal of Chemical Health Risks, 2021. **11**(4): p. 393-402.
34. Saha, P. and S. Chowdhury, *Insight into adsorption thermodynamics*. Thermodynamics, 2011. **16**: p. 349-364.
35. Kakavandi, B., A. Esrafil., A. Mohseni., Bandpi., *Magnetic Fe₃O₄@ C nanoparticles as adsorbents for removal of amoxicillin from aqueous solution*. Water science and technology, 2014. **69**(1): p. 147-155.
36. Khan, I., K. Saeed, and I. Khan, *Nanoparticles: Properties, applications and toxicities*. Arabian journal of chemistry, 2019. **12**(7): p. 908-931.

References

37. Kudr, J., Y .Haddad., L. Richtera., Z Heger., M. Cernak., *Magnetic nanoparticles: From design and synthesis to real world applications*. Nanomaterials, 2017. **7**(9): p. 243.
38. Mohammed, L., H.G. Goma., D. Ragab., J. Zhu., *Magnetic nanoparticles for environmental and biomedical applications: A review*. Particuology, 2017. **30**: p. 1-14.
39. Hu, M., H.J. Butt., K. Landfester., M.B. Bannwarth., S. Wooh., *Shaping the assembly of superparamagnetic nanoparticles*. ACS nano, 2019. **13**(3): p. 3015-3022.
40. Chomoucka, J., J .Drbohlovova., D. Huska., V. Adam., *Magnetic nanoparticles and targeted drug delivering*. Pharmacological research, 2010. **62**(2): p. 144-149.
41. Khojastehnezhad, A., B. Maleki., B. Karrabi., *Synthesis of highly functionalized piperidines using polyphosphoric acid supported on silica-coated magnetic nanoparticles*. Organic Preparations and Procedures International, 2017. **49**(4): p. 338-345.
42. Ali, A., H. Zafar., M. Zia., I. ul Haq., A.R. Phull., *Synthesis, characterization, applications, and challenges of iron oxide nanoparticles*. Nanotechnology, science and applications, 2016. **9**: p. 49.
43. Machala, L., J. Tucek, and R. Zboril, *Polymorphous transformations of nanometric iron (III) oxide: a review*. Chemistry of materials, 2011. **23**(14): p. 3255-3272.
44. Samrot, A.V., C.S. Sahithya., J. Selvarani. A., *Surface-engineered superparamagnetic iron oxide nanoparticles for chromium removal*. International journal of nanomedicine, 2019. **14**: p. 8105.
45. Sun, S. N., C. Wei., Z.Z. Zhu., Y.L. Hou., *Magnetic iron oxide nanoparticles: Synthesis and surface coating techniques for biomedical applications*. Chinese Physics B, 2014. **23**(3): p. 037503.
46. Wolf, E.L. and M. Medikonda, *Understanding the nanotechnology revolution*. 2012: John Wiley & Sons.
47. Bhandari, R., P. Gupta., T. Dziubla., J.Z. Hilt., *Single step synthesis, characterization and applications of curcumin functionalized iron oxide magnetic nanoparticles*. Materials Science and Engineering: C, 2016. **67**: p. 59-64.
48. Gahrouei, Z.E., M. Imani., M. Soltani., *Synthesis of iron oxide nanoparticles for hyperthermia application: effect of ultrasonic irradiation assisted co-precipitation route*. Advances in Natural Sciences: Nanoscience and Nanotechnology, 2020. **11**(2): p. 025001.
49. Akhtar, K., K. Javed, and S.S. Ali Shah, *Synthesis routes for multi-shape Fe₃O₄ nanoparticles through oxidation-precipitation of hematite and modified co-precipitation method without surfactant*. Journal of Dispersion Science and Technology, 2022: p. 1-11.
50. Tartaj, P., M.P. Morales., *Synthesis, properties and biomedical applications of magnetic nanoparticles*. Handbook of magnetic materials, 2006. **16**(5): p. 403-482.
51. Silva, M.F., L.A.S. De. Oliveira., M.A. Ciciliati., *The effects and role of polyvinylpyrrolidone on the size and phase composition of Iron oxide nanoparticles prepared by a modified sol-gel method*. Journal of Nanomaterials, 2017. **2017**.
52. Arshad, M., H.A. Siddiqui., S. Anjum., *Synthesis of iron oxide magnetic nanoparticle by sol-gel method and their characterization*. Professor Dr. Muhammad Tufail Convener, 2016. **98**: p. 98.
53. Zhu, M. and G. Diao, *Synthesis of porous Fe₃O₄ nanospheres and its application for the catalytic degradation of xylenol orange*. The Journal of Physical Chemistry C, 2011. **115**(39): p. 18923-18934.

References

54. Li, X., Z. Si., Y. Lei., J. Tang., S. Wang., S. Su., S. Song., *Direct hydrothermal synthesis of single-crystalline triangular Fe₃O₄ nanoprisms*. CrystEngComm, 2010. **12**(7): p. 2060-2063.
55. Ansari, M.O., M. Ahmad., N. Parveen., S. Ahmad., *Iron oxide nanoparticles-synthesis, surface modification, applications and toxicity: a review*. Materials Focus, 2017. **6**(3): p. 269-279.
56. Unni, M., A.M. Uhl., S. Savliwala., B.H. Savitzky., *Thermal decomposition synthesis of iron oxide nanoparticles with diminished magnetic dead layer by controlled addition of oxygen*. ACS nano, 2017. **11**(2): p. 2284-2303.
57. Konieczka, P., *Validation and regulatory issues for sample preparation in: comprehensive sampling and sample preparation*. 2012.
58. Ghime, D., T. Mohapatra., A. Verma., *Photodegradation of aqueous eosin yellow dye by carbon-doped TiO₂ photocatalyst*. in *IOP Conference Series: Earth and Environmental Science*. 2020. IOP Publishing.
59. Derayea, S.M. and D.M. Nagy, *Application of a xanthene dye, eosin Y, as spectroscopic probe in chemical and pharmaceutical analysis; a review*. Reviews in Analytical Chemistry, 2018. **37**(3).
60. Bello, O.S., O.A. Olusegun, and V.O. Njoku, *Fly ash: an alternative to powdered activated carbon for the removal of eosin dye from aqueous solutions*. Bulletin of the Chemical Society of Ethiopia, 2013. **27**(2): p. 191-204.
61. Ahmed, L.M., *Photo-decolourization kinetics of acid red 87 dye in ZnO suspension under different types of UV-A light*. Asian J. Chem, 2018. **30**(9): p. 2134-2140.
62. Ahmadi, S., C.H. Chia., S. Zakaria., K. Saeedfar., *Synthesis of Fe₃O₄ nanocrystals using hydrothermal approach*. Journal of Magnetism and Magnetic Materials, 2012. **324**(24): p. 4147-4150.
63. Hernandez, J.T., A.A. Muriel., J.A. Tabares., *Preparation of Fe₃O₄ nanoparticles and removal of methylene blue through adsorption*. in *Journal of Physics: Conference Series*. 2015. IOP Publishing.
64. Minitha, C.R., M. Martina Susan Arachy, and R.T. Rajendra Kumar, *Influence of Fe₃O₄ nanoparticles decoration on dye adsorption and magnetic separation properties of Fe₃O₄/rGO nanocomposites*. Separation Science and Technology, 2018. **53**(14): p. 2159-2169.
65. Rahmawati, R., A. Taufiq., S. Sunaryono., *Synthesis of magnetite (Fe₃O₄) nanoparticles from iron sands by coprecipitation-ultrasonic irradiation methods*. J. Mater. Environ. Sci, 2018. **9**(3): p. 155-160.
66. Liu, X., J. Tian., Y. Li., N. Sun., S. Mi., Y. Xie., Z. Chen., *Enhanced dyes adsorption from wastewater via Fe₃O₄ nanoparticles functionalized activated carbon*. Journal of hazardous materials, 2019. **373**: p. 397-407.
67. Takai, Z.I., M.K. Mustafa., S. Asman., *Preparation and characterization of magnetite (Fe₃O₄) nanoparticles by sol-gel method*. Int. J. Nanoelectron. Mater, 2019. **12**: p. 37-46.
68. Joshi, S., V.K. Garg., N. Kataria., K. Kadirvelu., *Applications of Fe₃O₄@ AC nanoparticles for dye removal from simulated wastewater*. Chemosphere, 2019. **236**: p. 124280.
69. Narayanaswamy, V., H. Kumar., C. Srivastava., *Adsorption of methylene blue and rhodamine B on graphene oxide-Fe₃O₄ nanocomposite: Molecular dynamics and Monte Carlo simulations*. Materials Express, 2020. **10**(3): p. 314-324.
70. Lesiak, B., N. Rangam., P. Jiricek., I. Gordeev., J. Toth., *Surface study of Fe₃O₄ nanoparticles functionalized with biocompatible adsorbed molecules*. Frontiers in chemistry, 2019. **7**: p. 642.

References

71. Jawad, T.M. and L.M. Ahmed, *Direct ultrasonic synthesis of WO₃/TiO₂ nanocomposites and applying them in the photo decolorization of eosin yellow dye*. Periodico Tche Quimica (Online), 2020. **17**(34): p. 621-633.
72. Fakhri, F.H. and L.M. Ahmed, *Incorporation CdS with ZnS as composite and using in photo-decolorization of congo red dye*. Indonesian Journal of Chemistry, 2019. **19**(4): p. 936-943.
73. Islam, A., *Preparation of mixed manganese oxide nano-matrix and studies on its oxidative and pathogenic activities*. 2015.
74. Karaj, I., *Raw and modified rice husk performance in removal of Basic Blue 41 from aqueous solutions*. Journal of Occupational and Environmental Health, 2016. **1**(1): p. 41-49.
75. Chikwe, T.N., R.E. Ekpo, and I. Okoye, *Competitive adsorption of organic solvents using modified and unmodified calcium bentonite clay mineral*. Chem. Int, 2018. **4**(4): p. 230-239.
76. Ocana, M., *Uniform particles of manganese compounds obtained by forced hydrolysis of manganese (II) acetate*. Colloid and polymer science, 2000. **278**(5): p. 443-449.
77. Kang, L., M. Zhang., Z.H. Liu., K. Ooi., *IR spectra of manganese oxides with either layered or tunnel structures*. Spectrochimica Acta Part A: Molecular and Biomolecular Spectroscopy, 2007. **67**(3-4): p. 864-869.
78. Luo, X., S. Liu., J. Zhou., L. Zhang., *In situ synthesis of Fe₃O₄/cellulose microspheres with magnetic-induced protein delivery*. Journal of Materials Chemistry, 2009. **19**(21): p. 3538-3545.
79. Ramesh, A., D. Rama. Devi., S. Mohan. Botsa., *Facile green synthesis of Fe₃O₄ nanoparticles using aqueous leaf extract of Zanthoxylum armatum DC. for efficient adsorption of methylene blue*. Journal of Asian Ceramic Societies, 2018. **6**(2): p. 145-155.
80. Ahmed, L.M., F.H. Hussein, and A.A. Mahdi, *Photocatalytic dehydrogenation of aqueous methanol solution by naked and platinized TiO₂ nanoparticles*. Asian Journal of Chemistry, 2012. **24**(12): p. 5564.
81. Kadhim, H., L. Ahmed, and M. AL-Hachamii, *Facile Synthesis of Spinel CoCr₂O₄ and Its Nanocomposite with ZrO₂: Employing in Photo-catalytic Decolorization of Fe (II)-(luminol-Tyrosine) Complex*. Egyptian Journal of Chemistry, 2022. **65**(1): p. 481-488.
82. Obaid, A. and L. Ahmed, *One-step hydrothermal synthesis of α-MoO₃ nano-belts with ultrasonic assist for incorporating TiO₂ as a nanocomposite*. Egyptian Journal of Chemistry, 2021. **64**(10): p. 5725-5734.
83. Hayawi, M.K., L.M. Ahmed, and M.M. Kareem, *Synthesis of spinel Mn₃O₄ and spinel Mn₃O₄/ZrO₂ nanocomposites and using them in photo-catalytic decolorization of Fe (II)-(4, 5-diazafluoren-9-one 11) complex*. Periodico Tche Quimica (Online), 2020. **17**(34): p. 689-699.
84. Karam, F.F., N.H.M. Saeed., A. Al. Yasasri., *Kinetic study for reduced the toxicity of textile dyes (reactive yellow 14 dye and reactive green dye) using UV-A Light/ZnO system*. Egyptian Journal of Chemistry, 2020. **63**(8): p. 2987-2998.
85. Cornell, R.M. and U. Schwertmann, *The iron oxides: structure, properties, reactions, occurrences, and uses*. Vol. 664. 2003: Wiley-vch Weinheim.
86. Ulu, A., S.A.A. Noma., S. Koytepe., B. Ates., *Magnetic Fe₃O₄@ MCM-41 core-shell nanoparticles functionalized with thiol silane for efficient l-asparaginase immobilization*. Artificial cells, nanomedicine, and biotechnology, 2018. **46**(sup2): p. 1035-1045.

References

87. Guo, W., Z. Fu., Z. Zhang., H. Wang., S. Liu., W. Feng., *Synthesis of Fe₃O₄ magnetic nanoparticles coated with cationic surfactants and their applications in Sb (V) removal from water*. Science of The Total Environment, 2020. **710**: p. 136302.
88. Lu, T., J. Wang., J. Yin., A. Wang., X. Wang., *Surfactant effects on the microstructures of Fe₃O₄ nanoparticles synthesized by microemulsion method*. Colloids and Surfaces A: Physicochemical and Engineering Aspects, 2013. **436**: p. 675-683.
89. Mall, I.D., V.C. Srivastava, and N.K. Agarwal, *Removal of Orange-G and Methyl Violet dyes by adsorption onto bagasse fly ash—kinetic study and equilibrium isotherm analyses*. Dyes and pigments, 2006. **69**(3): p. 210-223.
90. Suzuki, M. and M. Suzuki, *Adsorption engineering*. Vol. 14. 1990: Kodansha Tokyo.
91. Purkait, M., S. DasGupta, and S. De, *Adsorption of eosin dye on activated carbon and its surfactant based desorption*. Journal of environmental management, 2005. **76**(2): p. 135-142.
92. Skoog, D.A., D.M. West., F.J. Holler., S.R. Crouch., *Fundamentals of analytical chemistry*. 2013: Cengage learning.
93. Zhu, Y., Q. Yang., T. Lu., W. Qi., H. Zhang., M. Wang., *Effect of phosphate on the adsorption of antibiotics onto iron oxide minerals: Comparison between tetracycline and ciprofloxacin*. Ecotoxicology and Environmental Safety, 2020. **205**: p. 111345.
94. Sadeghi, M., M. Irandoust., F. Khorshidi., M. Feyzi., *Removal of Arsenic (III) from natural contaminated water using magnetic nanocomposite: kinetics and isotherm studies*. Journal of the Iranian Chemical Society, 2016. **13**(7): p. 1175-1188.
95. Hussain, Z.A., F.H. Fakhri., H.F. Alesary., *ZnO Based Material as Photocatalyst for Treating the Textile Anthraquinone Derivative Dye (Dispersive Blue 26 Dye): Removal and Photocatalytic Treatment*. in *Journal of Physics: Conference Series*. 2020. IOP Publishing.
96. Zarrouk, A., B. Hammouti., H. Zarrok., *Temperature effect, activation energies and thermodynamic adsorption studies of L-cysteine methyl ester hydrochloride as copper corrosion inhibitor in nitric acid 2M*. Int. J. Electrochem. Sci, 2011. **6**(12): p. 6261-6274.
97. Tang, H., W. Zhou, and L. Zhang, *Adsorption isotherms and kinetics studies of malachite green on chitin hydrogels*. Journal of hazardous materials, 2012. **209**: p. 218-225.
98. Piccin, J., C.S. Gomes., L.A. Feris., M. Gutterres., *Kinetics and isotherms of leather dye adsorption by tannery solid waste*. Chemical Engineering Journal, 2012. **183**: p. 30-38.

الخلاصة

يشتمل هذا العمل على ثلاثة خطوط ، الخط الاول تم باستخدام تقنية ترسيب مبتكره لتحضير جزيئات Fe_3O_4 النانوية المغناطيسية بوجود الاوكسجين الجوي بدون ومع استخدام مواد مختلفة خافضة للتوتر السطحي كقوالب، بما في ذلك كبريتات دوديسيل الصوديوم (SDS) ، تريتون X100 ، بروميد سيتريمونيوم (CTAB) ، وسيتراميد (CT). حضرت جزيئات أكسيد الحديد المغناطيسي (Fe_3O_4) النانوية على شكل إسيبنيل معكوس ($Fe_2O_3 \cdot FeO$)، عند دمج محلول كبريتات الحديد مع خليط مائي من هيدروكسيد الصوديوم ونترات الصوديوم التحضير بدون أي كلسنة تحت جو من غاز الأوكسجين.

من خلال خط العمل الثاني، تم التعرف على جزيئات أكسيد الحديد النانوية ($Spinel Fe_3O_4$) باستخدام عدة تقنيات، بما في ذلك التحليل الطيفي بالأشعة تحت الحمراء (FTIR) ، وتحليل حيود الأشعة السينية (XRD)، ومجهر المسح الإلكتروني (SEM). اذ أظهر تحليل طيف الأشعة تحت الحمراء قممًا مميزة عند 744-598 cm^{-1} ، مما يؤكد وجود هياكل رباعية السطوح وثمانية السطوح لجسيمات أكسيد الحديد النانوية المحضرة باعتبارها الإسيبنيل المعكوس. أوضح حيود الأشعة السينية أن العينات المحضرة بدون ومع العوامل الخافضة للتوتر السطحي هي بلورية بطبيعتها، وتراوح حجمها النانوي من (8.5 نانومتر بدون مواد خافضة للتوتر السطحي إلى 27.72 نانومتر باستخدام المواد الخافضة للتوتر السطحي). اظهرت صور ال SEM لجسيمات أكسيد الحديد النانوية المحضرة بدون وباستخدام مواد خافضة للتوتر السطحي انها ذات أشكالاً كروية متجمعه بهيئة مقاطع شبه منتظمة ذات هياكل نانوية تشبه البروكلي.

من ناحية أخرى من خلال الخط الثالث للعمل، استخدامات جزيئات أكسيد الحديد النانوية كمادة مازة لإزالة صبغة الايوسين الصفراء من المحاليل المائية. في البداية تم إجراء تجربة امتزاز لجميع الأسطح المحضرة باتجاه الصبغة، حيث وجد أن أفضل نسبة إزالة للصبغة كانت على سطح جزيئات أكسيد الحديد النانوية مع السيتريميد ($Fe_3O_4+cetramide$) ، حيث وصلت نسبة الإزالة إلى 94.7%.

بعد ذلك تمت دراسة العوامل المؤثرة على عملية الامتزاز لسطح اوكسيد الحديد باستخدام السيتريميد فقط ، وقد أعطى Fe_3O_4 المحضر بالسيتريميد كفاءة إزالة أعلى مقارنة بأكاسيد الحديد المحضرة. وجد ان سعة الامتزاز تزداد بزيادة زمن الاتزان حتى تصل لمرحلة التشبع (الاتزان) بزمن 60 دقيقة. بينما أثناء اختبار تأثير كمية السطح على عملية الامتزاز ظهرت

زيادة في كفاءة الإزالة مع زيادة كتلة السطح نتيجة لزيادة مساحة السطح ، وكان امتزاز الصبغة بشكل أكثر فاعلية عند وزن 0.01 غم. أظهر عامل الأس الهيدروجيني تأثيرًا واضحًا على الإزالة ، حيث وجد أن أفضل إزالة للصبغة في وسط متعادل (الرقم الهيدروجيني 6.5) وذلك يرجع إلى وجود مجموعات معادلة في تكوين الصبغة الصفراء.

من ناحية أخرى ، وجد أن كفاءة الإزالة تزداد مع زيادة درجة الحرارة نتيجة لزيادة الطاقة الحركية ، مما يسهل وصول جزيئات الصبغة إلى المواقع النشطة على سطح الممتزات. كما أظهرت الدراسة الديناميكية الحرارية أن عملية امتزاز جزيئات أكسيد الحديد النانوي مع السيتريميد هي عملية ماصة للحرارة حيث أن المحتوى الحراري موجب وتلقائي ولا يتطلب مصدر خارجي وعلى العكس من ذلك أن عملية امتزاز جزيئات أكسيد الحديد النانوي بغياب السيتريميد هي عملية باعثة للحرارة حيث أن المحتوى الحراري سالب وغير تلقائي.

يخضع المغنتيت مع السيتراميد للامتزاز الكيميائي لأن الانثالي لهذا التفاعل أكثر قيمة من (20) كيلو جول \ مول في المقابل فإن Fe_3O_4 في حالة عدم وجود السيتريميد يخضع لامتزاز فيزيائي لأن قيمة الانثالي أقل من (20) كيلو جول \ مول.

كما اظهرت البيانات المأخوذة من معادلات نموذج الأيزوثرم أن المغنتيت الناتج بوجود السيتراميد يخضع الى معادلات لانجموير وفريوندليش وتيمكن بينما لا ينطبق Fe_3O_4 المتكون في حالة عدم وجود سيتراميد.



جامعة كربلاء
كلية العلوم
قسم الكيمياء

تحضير وتوصيف جزيئات أكسيد الحديد النانوية واستخدامها في إزالة الا يوسين الصفراء من المحاليل المائية صبغة

رسالة مقدمة الى مجلس كلية العلوم / جامعة كربلاء وهي جزء من متطلبات نيل درجة
الماجستير في علوم الكيمياء

من قبل

حسين مهاوش محمد

بإشراف

أ. د لى مجيد احمد

أ.م.د شيماء ابراهيم سعيد